A Vibrating Edge Supported Plate, Fabricated by the Methods of Micro Electro Mechanical System for the Simultaneous Measurement of Density and Viscosity: Results for Methylbenzene and Octane at Temperatures between (323 and 423) K and Pressures in the Range (0.1 to 68) MPa

Anthony R. H. Goodwin,* Eric P. Donzier, and Olivier Vancauwenberghe

Schlumberger-Doll Research, 36 Old Quarry Road, Ridgefield, Connecticut 06877

Alistair D. Fitt and Kelly A. Ronaldson

School of Mathematics, University of Southampton, Highfield, Southampton SO17 1BJ, U.K.

William A. Wakeham

School of Engineering Sciences, University of Southampton, Highfield, Southampton SO17 1BJ, U.K.

Maria Manrique de Lara

Schlumberger Cambridge Research, High Cross, Madingley Road, Cambridge CB3 0EL, U.K.

Frederic Marty and Bruno Mercier

École Supérieure d'Ingénieurs en Électrotechnique et Électronique, Cité Descartes, 2 Boulevard Blaise Pascal, BP 99, 93162 Noisy le Grand, France

In the petroleum industry, measurements of the density and viscosity of petroleum reservoir fluids are required to determine the value of the produced fluid and production strategy. These thermophysical properties are also useful for the design of separators and process equipment and to control production processes. To measure the density and viscosity of petroleum fluids requires a transducer that can operate up to reservoir conditions and, to guide value and exploitation calculations with sufficient rigor, provide results with an accuracy of about ± 1 % in density and ± 10 % in viscosity. Necessarily, these specifications place robustness as a superior priority to accuracy for the design. In this paper, we describe a Micro Electrical Mechanical System (MEMS) that is capable of providing both density and viscosity of fluids in which it is immersed at the desired operating conditions. This transducer is based on a vibrating plate, with dimensions of about 1 mm and mass of about 0.12 mg, clamped along one edge. The measured resonance frequency of the first bending mode in a vacuum at a temperature of 298 K is about 12 kHz with a quality factor about 2600. Measurements of the resonance frequency and quality factor of the first-order bending mode were combined with semiempirical working equations and the mechanical properties of the plate to determine the density and viscosity when immersed in methylbenzene at temperatures of (323 and 373) K and octane at temperatures between (323 and 423) K both at pressures below 68 MPa where the density varies between (619 and 890) kg·m^{-3} and the viscosity varies from (0.205 to 0.711) mPa·s. The measurements in methylbenzene at pressures between (0.1 and 68) MPa and a temperature of 323 K were used to determine the adjustable parameters in the semiempirical working equations. The expanded ($k = 2$) (twice the standard deviation) uncertainty, including the calibration, in density is about ± 0.2 % and in viscosity is about ± 2.5 %; at a temperature of 423 K, the expanded uncertainty in viscosity is about 6 %. The results obtained at temperatures below 423 K differed by less than ± 0.3 % for density and less than ± 5 % for viscosity from either accepted correlations of literature values or results documented by others with experimental techniques that utilize different principles and have quite different sources of systematic error. These differences are within a reasonable multiple of the relative combined expanded uncertainty of our measurements. For octane at a temperature of 423 K, the measured viscosity differed by less than 13 % from literature values while the density differed by less than ± 0.5 %.

Introduction

The evaluation of the economic viability of a hydrocarbon-bearing formation requires measurements of many physical properties of both the porous medium and the fluid. In particular, the thermophysical properties of hydrocarbon reservoir fluids are required to determine flow in porous media and design completion, separation, treating, and metering systems. The financial analysis that determines the potential for commercial benefit from exploitation of naturally occurring hydrocarbon

* Corresponding author present address: Schlumberger, 125 Industrial Blvd, Sugar Land, TX 77478. Telephone: (281)285-4962. Fax: (281)285-8071. E-mail: agoodwin@slb.com.

10.1021/je0503296 CCC: $33.50
Published on Web 12/10/2005

resources is determined from knowledge of the reservoir permeability, size, shape, and compartmentalization and the fluid thermophysical properties. The uncertainty in viscosity, density, and phase behavior of the petroleum fluid impact the financial analysis. To a first approximation, measurements of density provide an estimate of the commercial value of the produced fluid while viscosity is an indicator of the ease with which the fluid can be extracted from the formation. Viscosity is arguably the single most important property.

A complete reservoir typically consists of a group of fluid-bearing layers separated by impermeable shale. The physical properties of the fluids can be determined from measurements performed on a subsample of an aliquot extracted from each layer (usually referred to as a zone). Often the extraction is performed after the borehole has been drilled but before the production system, consisting of metal tubes surrounded by cement, is installed. From samples collected down-hole, all physical properties of the fluid can be determined in a laboratory at reservoir temperature as well as the variations with temperature and pressures that will be experienced throughout the production system. These measurements are combined with knowledge of the permeability of the reservoir and the reservoir size, shape, and compartmentalization to perform analyses concerning the development of that petroleum reservoir. From this list, the thermophysical properties and their uncertainty are usually considered to be lower in priority than the other items in the financial analysis. However, uncertainties in the thermophysical properties, particularly for retrograde condensates, that arise from the operating conditions (reservoir conditions as well as temperatures and pressures experienced throughout the production system) and sampling techniques can be significant and may be reduced by direct measurement. In general, such measurements of density and viscosity with uncertainties of about $\pm$ 1 % and $\pm$ 10 %, respectively, are considered adequate to guide value and exploitation calculations with sufficient rigor. Thus, methods that can provide in situ measurements of fluid density and viscosity with these uncertainties at reservoir temperature are desirable because they reduce the time required for analysis and systematic errors that might arise from variations in chemical composition caused by transferring the fluids from one container to another and subsequent transportation.

There are numerous methods by which the viscosity of liquids can be measured. These have been reviewed by Johnson et al.,[1] Künzel et al.,[2] Nieuwoudt and Shankland,[3] and Kawata et al.[4,5] Vibrating objects including the vibrating wire and torsional viscometers were described by Diller and van der Gulik.[6] Wagner et al.,[7] Wagner and Kleinrahm,[8] and Kuramoto et al.[9] all described methods of determining liquid densities while Fujii[10,11] described absolute density standards. Majer and Pádua[12] and Stansfeld[13] discussed vibrating body densimeters. Other methods have been proposed to measure viscosity; for example, a vibrating tube[14] and techniques other than a vibrating wire[12] have been implemented to measure both viscosity and density, such as those utilizing ultrasonic plate waves[15] and bubble-rise speed.[16] Of the numerous methods that have been reported to measure density and viscosity, the most relevant to the transducer discussed in this paper are those that utilize a vibrating object of defined geometry and are fabricated by the methods of Micro Electro Mechanical System (MEMS). To our knowledge, the instrument reported by Woodward[17] is the earliest example of a vibrating object that is conceptually similar to the device described here. In ref 17, a 0.25 mm thick steel disk of diameter about 5 mm was connected via a narrow neck to a clamp. The disk was forced to vibrate, and measurements of resonance were used to determine the product of the density and viscosity. The archival literature contains many articles reporting transducers for the measurement of density and viscosity that are fabricated by the methods of MEMS. Of those numerous articles we, arbitrarily, provide the following four examples: Andrews and Harris[18] report a transducer with two parallel plates, each supported by beams, that are oscillated normal to each other to determine the viscosity of gases; Martin et al.[19] used a flexural plate wave resonator, fabricated on a silicon nitride membrane, to determine density; the ultrasonic plate wave resonator reported in ref 15 used a MEMS fabricated on a silicon carbide substrate; and, vibrating U-tube densimeters fabricated with MEMS albeit with square rather than the traditional circular cross-section.[20−22] In addition to these devices, there are numerous applications of cantilever beams (developed from the devices used in atomic force microscopy[23]) to the measurement of density and viscosity.[24−33] The width and length of the cantilevers vary from about (2 to 200) $\cdot 10^{-6}$ m with a thickness of order $1 \cdot 10^{-6}$ m.[34] The instruments described in refs 27 and 29 used a cantilever, exposed to air, to excite and detect the motion of a $50 \cdot 10^{-6}$ m diameter silica sphere immersed within a fluid. The sphere was connected to the cantilever by a $50 \cdot 10^{-6}$ m diameter silica rod. Cantilever beams have also been used to study the Knudsen effect,[35] determine flow rates,[36] measure the mechanical properties of electroplated gold films,[37] determine Young's modulus,[38,39] and form chemical[40−44] and biochemical[45−47] sensors.[48] For the chemical and biochemical sensors, the species to be detected is adsorbed on a chemically functionalized surface as this is detected through either variations in resonance frequency that is attributed to an added mass[40] or deflection of the beam arising from a variation in surface stress.[45,49,50]

Selecting a particular sensor system for a specific application requires consideration and weighting of each design, implementation, and fabrication method. Shieh et al.[51] have described systematic methods to select the most appropriate sensor for a particular application including devices that are based on coupled electromechanical phenomena. The essence of their approach relies on matching the desired sensor operating characteristics with the requirements of the desired application. These philosophical processes are even more crucial when no off-the-shelf commercial sensor is available. In this case, a sensor must be developed by carefully matching the requirements to the potential characteristics of the sensor. Our application requires operation at reservoir conditions with accuracy in density and viscosity of about $\pm$ 1 % and $\pm$ 10 %, respectively, that are adequate for calculations concerning the exploitation of petroleum reserves. Typically, the reservoir and production system have temperatures less than 473 K at pressures below 200 MPa. Transducers that are operated in the bore-hole have historically placed robustness as a superior priority to accuracy in the design process, and this is the case for the sensor presented here. The design, fabrication, and application of MEMS sensors has been discussed by Judy,[52] while Werner and Fahrner[53] have reviewed devices, fabricated from silicon, that were specifically intended for operation at high temperature and in harsh environments similar to those found in petroleum reservoirs.

To develop a method for the in situ and simultaneous measurement of density and viscosity, we have chosen to construct a vibrating object. The transducer described in this paper (shown in Figure 1) is similar to a cantilever in that it is a rectangular plate connected to a support along one edge.

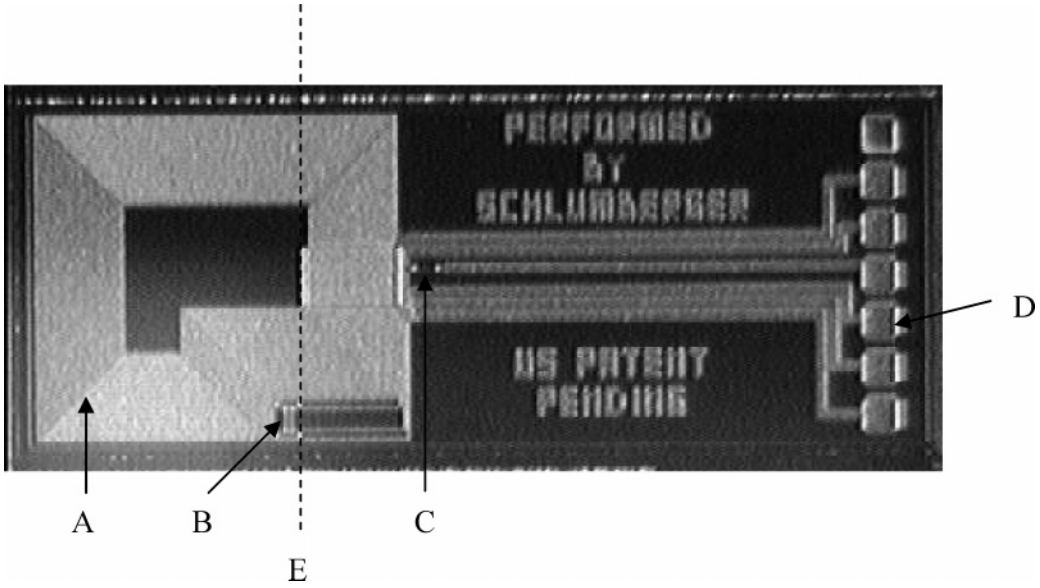

Figure 1. Photograph of the top surface of the MEMS showing the aluminum coil A, Wheatstone bridge B, boron-doped polycrystalline silicon resistor that acted as thermometer C, and wire-bond pads D. The $\approx 22.25 \cdot 10^{-6}$ m thick plate is to the left of dashed line E, and to the right of the dashed line the MEMS has an additional $\approx 350 \cdot 10^{-6}$ m thick monocrystalline silicon beneath.

However, our device has a width of about 2 mm, a length of about 1.5 mm, and a thickness of about $20 \cdot 10^{-6}$ m. The density and viscosity of the fluid in which the plate is immersed has been determined from measurements of the first, non-zero frequency, eigenmode, which is a symmetrical bending mode with flexural motion. The design of the edge-supported vibrating plate densimeter/viscometer described here and shown in Figure 1 is based on a magnetic field sensor originally reported by Donzier et al.[54] and fabricated by the methods of MEMS. The object developed for this work was fabricated from monocrystalline silicon, a mechanically stable material, by addition of layers to produce a means of exciting and detecting the motion of the plate near resonance. This MEMS sensor utilizes silicon-on-insulator (SOI) wafers, photolithography (as used in integrated circuit fabrication), and deep reactive ion etching for the micro-machining. A physical description of the motion of the plate in a fluid, which is used to obtain density and viscosity, requires a geometrically defined structure of known dimensions. When the sensor is formed by the methods of MEMS, this requirement necessarily precludes the use of curved surfaces. The MEMS densimeter/viscometer described here is one of five devices that have been fabricated by us to measure density, viscosity, relative permittivity, thermal conductivity, and heat capacity.

When the MEMS fabricated device (illustrated in Figure 1) is placed in a fluid, to a first approximation its resonance frequency f_r and quality factor Q ($= f_r/2g$) decrease with increasing density and viscosity, respectively. To define the parameter g, we determine the frequencies ($f_r - g$) and ($f_r + g$) above and below the resonance frequency (f_r) at which the measured amplitude is equal $A_{max}/2^{1/2}$ where A_{max} is the maximum amplitude at f_r. The general effect of the fluid on the plate can be understood by two albeit naive approximations. First, the resonant frequency decreases with increasing density because of added mass. Second, Q decreases as the viscosity increases owing to the shearing motion at the tip of the plate. Indeed, the methods of MEMS have provided a means of constructing a densimeter that has a resonance frequency sensitive to the added mass of fluid in which it is immersed. This arises because the plate has a large surface-to-volume ratio and mass of about 0.12 mg. The plate mass is equal to the mass of octane at $T = 323$ K and $p = 0.1$ MPa contained in about five viscous skin depths [for fluid density ρ and viscosity η given by $\delta = \{\eta/(\rho\pi f)\}^{1/2}$, for octane under these conditions $\delta = 7.3 \cdot 10^{-6}$ m] around the plate when the plate resonates at a frequency of about 3.4 kHz.

Typically, petroleum reservoir fluids have densities in the range (300 to 1300) kg·m^{-3} and viscosities between (0.05 to 1 000) mPa·s. For recoverable and Newtonian hydrocarbon liquids (fluids that are at a pressure of 0.1 MPa), the density is within the range (700 to 1000) kg·m^{-3} while the viscosity is between (0.5 and 100) mPa·s. Newtonian fluids of known viscosities and densities, that include at least the ranges defined for hydrocarbon liquids, are required for the laboratory evaluation of proposed in situ measurement techniques and calibration of other viscometers and densimeters as a function of both temperature and pressure.[55−57] In this paper we are concerned solely with fluids that are Newtonian so that their viscosity is independent of the rate of shear, and we present results for methylbenzene at densities between (805 and 890) kg·m^{-3} and viscosities in the range (0.293 to 0.658) mPa·s and for octane at densities between (619 and 734) kg·m^{-3} and viscosities in the range (0.205 to 0.711) mPa·s. In another paper, we report measurements when a similar MEMS densimeter/viscometer was surrounded by argon at densities between (79 and 767) kg·m^{-3} and viscosities in the range (26 to 57) $\cdot 10^{-6}$ Pa·s.[58] Non-Newtonian fluids are also encountered in the production of petroleum, for example, drilling lubricants with additives such as sodium bentonite that increase the density. A transducer suitable for operation in both Newtonian and non-Newtonian fluids is the subject of another paper;[59] we anticipate for the Newtonian fluid case that the device will provide the product of density and viscosity.

In a future paper, we will present measurements when the MEMS densimeter/viscometer has been exposed to fluids with densities in the range (1 to 1 850) kg·m^{-3}, where the frequency decreased from $\approx$ (12 to 3) kHz with increasing density, and viscosities that varied from (0.010 to 300) mPa·s, where the resonance quality factor decreased from $\approx$ (100 to 1.5) with increasing viscosity.

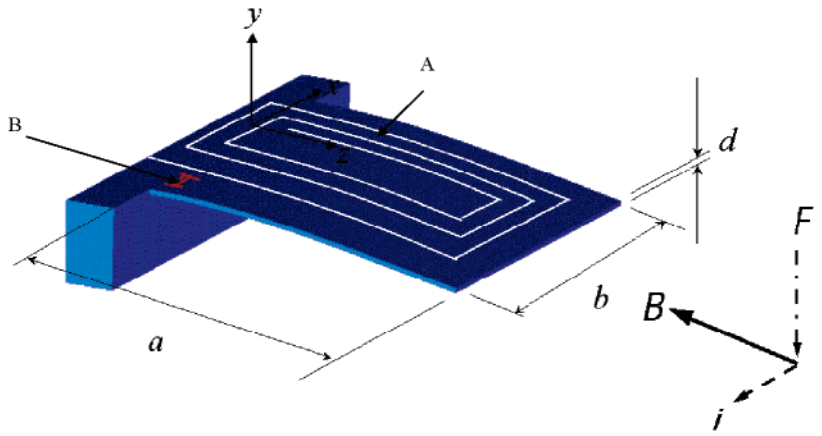

Figure 2. Isometric projection of a MEMS plate of length *a*, width *b*, and thickness *d* illustrating the relative positions of the applied magnetic flux *B*, the direction of the current *i* through the coil A, and the resulting force *F* creating a motion in the *y* plane detected by the Wheatstone bridge B.

Theory

Lindolm et al.[60] and Leissa[61] have presented theoretical descriptions of the elastic vibration of plates, but neither ref 60 nor ref 61 provide working equations suitable for the plate and application considered in this study. However, models have been reported for the response of a cantilever beam immersed directly in a fluid.[24−26,28,31−33,40,62−66] The majority of these models for the flexural response amount to an added mass with a damping coefficient[17,24,25,28,31−33,40,62−65] and have included experimental verification[66] of the models, internal damping,[67] and temperature dependence of the sensitivity to external force.[68] The added mass model for the flexural response reported by Sadar[63] is based on an expression reported by Lindolm et al.[60] and has been extended to also include torsional oscillation.[69] Cantilever beams, exposed to air, have also used to actuate and detect the motion of a sphere immersed in a fluid and the response of the coupled cantilever and sphere interpreted with adaptations of an expression presented by Landau and Lifshitz[70] for the oscillation of a sphere immersed in a fluid.[27,29,71] Cumberbatch and co-workers[72,73] presented a model for an elastic solid plate clamped on two opposite sides vibrating in an inviscid fluid to describe a commercially available densimeter.[13]

To model the response of the edge-supported plate oscillating while immersed in a fluid, we have adopted an approach similar to that described in refs 72 and 73 and modeled our edge-supported plate by decoupling the effects of viscosity and density so that the density is determined solely from the resonance frequency and, at least in this paper, introduced another independent equation for the product of viscosity and density. Because of the secondary emphasis placed on accuracy during the design, we anticipate the results of our measurements and conclude that these approximations are adequate for the target accuracy. However, if either higher accuracy in density and viscosity or operation over a wider range of density and viscosity are required, then the working equations presented here will not suffice even for the modest accuracy desired for the application described in the Introduction. For these cases, working equations will need to be formulated that couple both fluid flow and plate motion.

The MEMS plate is modeled as a one-dimensional beam (shown in Figure 2) supported at one end $y = z = 0$.[72,73] The transverse displacement of the plate normal to the (x, z) plane is denoted, as shown in Figure 2, by

$$y = q(x,z,t) \tag{1}$$

We assume that the longitudinal strain varies linearly across the plate's depth and that the bending moment at any cross section is proportional to a local radius of curvature. We will consider only the first eigenmode (1,0) (motion independent of x) and will also ignore plate edge effects. The displacement (q) is governed by the Euler−Bernoulli bending theory of thin plates so that

$$\rho_s d\frac{\partial^2 q}{\partial t^2} + \frac{Ed^3}{12(1-\sigma^2)}\nabla^4 q = F \tag{2}$$

where $\nabla^2 = \partial^2/\partial x^2 + \partial^2/\partial z^2$. In eq 2, we have $0 \le z \le a$, $-b/2 \le x \le b/2$, F denotes the force per unit area applied normal to the plate, a denotes the plate length, and b is the plate breadth. In eq 2, d is the plate thickness, E is Young's modulus, σ is Poisson's ratio, and ρ_s is the density of the plate material. We assume that the fluid is inviscid and incompressible (so that $\nabla\cdot v = 0$, where $\boldsymbol{v} = (u,v)$ is the fluid velocity), and that the flow is irrotational so that $v = \nabla\Phi$ where the velocity potential (Φ) satisfies

$$\frac{\partial\Phi}{\partial x} = u \tag{3}$$

$$\frac{\partial\Phi}{\partial y} = v \tag{4}$$

and

$$\nabla^2\Phi = 0 \tag{5}$$

Boundary conditions must now be proposed for eq 2. The pinned or simply supported condition has been used because the plate is formed from a series of layers and mounted to a printed circuit board within a tube that is filled with adhesive. (The specification of this boundary condition will be discussed further below.) At the supported end $z = 0$, this implies that the oscillating plate has neither deflection nor bending so that $q = \partial^2 q/\partial z^2 = 0$. At the free end of the plate $z = a$ there is neither bending nor shear force so that $\partial^2 q/\partial z^2 = \partial^3 q/\partial z^3 = 0$. We assume that, in vacuo, no force acts on the plate ($F = 0$) and that it oscillates with harmonic motion of the form $q = Z(z)e^{-i2\pi ft}$. We now note that the function

$$q(z,t) = \bar{A}\cos(2\pi ft)\left[\sin(v_n z/a) + \frac{\sin(v_n)}{\sinh(v_n)}\sinh(v_n z/a)\right] \tag{6}$$

(where $\bar{A}$ is an arbitrary constant) satisfies all the boundary conditions so long as the eigenvalues (v_n) are chosen so that

tan (v_n) = tanh (v_n): for the (1,0) mode $v_1 = 3.926602312$. Equation 6 further satisfies eq 2 with $F = 0$ provided $48\rho_s\pi^2 f^2 a^4(1 - \sigma^2) = Ed^2 v_n^4$.

The fluid flow must now be determined so that the force per unit area on the plate (F) that appears in eq 2 may be calculated. In general the fluid flow excited by the plate is extremely complicated, but we will simplify matters by assuming that both the plate thickness ($d \approx 2{\cdot}10^{-5}$ m) and the amplitude of the plate oscillations (see below) are small as compared to the plate dimensions $a \approx 1.5{\cdot}10^{-3}$ m and b. So-called "thin aerofoil theory"[74,75] may be invoked. Essentially this allows us to assume (a) that flow boundary conditions may be imposed on $y = 0$ rather than on the actual moving surface of the vibrating plate and (b) that the fluid normal velocity component (v) is equal to the rate of change of displacement of the plate with respect to time on $y = 0$. This considerably simplifies the potential flow problem that must be solved.

With the thin aerofoil theory assumptions, the velocity potential $\Phi = \Phi^+$ and $\Phi = \Phi^-$ (denoting the velocity potentials in the regions $y > 0$ and $y < 0$, respectively) must each satisfy Laplace's equation and in addition the boundary condition that

$$\frac{\partial q}{\partial t} = \frac{\partial \Phi}{\partial y} \tag{7}$$

on $y = 0$; preliminary measurements of the plate displacement as a function of distance from the support suggest that the maximum motion of the plate tip ($z = a$) is about 0.1 μm when immersed in a liquid. The force per unit area acting on the plate is given by

$$F = -[p(y > 0) - p(y < 0)] \tag{8}$$

For an inviscid fluid, the Bernoulli's equation (neglecting the gravity and the velocity terms, which may be confirmed to be negligibly small) gives the pressure as

$$p = -\rho_f \frac{\partial \Phi}{\partial t} \tag{9}$$

where ρ_f is the fluid density. Solutions of Laplace's equation that satisfy eq 7 are given by

$$\Phi^+ = \frac{2a\bar{A}\pi f \sin(2\pi ft)}{v_n}\left\{ e^{-v_n y/a}\sin(zv_n/a) + \frac{\sinh(zv_n/a)\sin(v_n)}{\sinh(v_n)}[\cos(yv_n/a) - \sin(yv_n/a)]\right\} \tag{10}$$

and

$$\Phi^- = -\frac{2a\bar{A}\pi f \sin(2\pi ft)}{v_n}\left\{ e^{v_n y/a}\sin(zv_n/a) + \frac{\sinh(zv_n/a)\sin(v_n)}{\sinh(v_n)}[\cos(yv_n/a) + \sin(yv_n/a)]\right\} \tag{11}$$

Using eqs 10 and 11 in eq 9 and then eq 8, we find that

$$F = \frac{8\rho_f a\bar{A}\pi^2 f^2 \cos(2\pi ft)}{v_n}\left[\sin(zv_n/a) + \frac{\sin(v_n)}{\sinh(v_n)}\sinh(zv_n/a)\right] \tag{12}$$

When this expression for F and the expression for q given by eq 6 are substituted into eq 2, we find after simplification that

$$\rho_f = \frac{Ev_n^5 d^3}{24\{1-\sigma^2\}a^5(2\pi f_{r,f})^2} - \frac{\rho_s d v_n}{2a} \tag{13}$$

where ρ_f is the fluid density and $f_{r,f}$ is the resonance frequency of the plate immersed in fluid. In a vacuum ($\rho_f = 0$), eq 13 reduces to

$$f_r(p=0) = (2\pi)^{-1}\left[\frac{Ev_n^4 d^2}{12\{1-\sigma^2\}a^4\rho_s}\right]^{1/2} \tag{14}$$

for the resonance frequency ($f_r(p = 0)$). We recall that in eqs 13 and 14 a is the plate length and d is the plate thickness. Both eqs 13 and 14 require values of Young's modulus (E), Possion's ratio (σ), and density of the material (ρ_s). Finally, it should be noted that a similar analysis can be carried out if, instead of the pinned condition $\partial^2 q/\partial z^2 = 0$ at $z = 0$, a "clamped" condition $\partial q/\partial z = 0$ is used: the only difference to the end result is that an additional multiplicative factor of 2 is present in the right-hand side of eq 13. The construction of the sensor makes it hard to determine which of these two conditions is the more appropriate: as shown below, the best results are obtained when a combination of the two conditions is used.

In this work, Young's modulus (E) and Poisson's ratio (σ) of silicon with crystallographic plane (1,0,0) (used to fabricate the transducer used in this work) were obtained from

$$E = (c_{11,S} + 2c_{12,S})(c_{11,S} - c_{12,S})/(c_{11,S} + c_{12,S}) \tag{15}$$

and

$$\sigma = c_{12,S}/(c_{11,S} + c_{12,S}) \tag{16}$$

with the temperature-dependent adiabatic stiffness elastic constants $c_{11,S}$ and $c_{12,S}$ obtained from a combination of the measurements reported by McSkimin[76] and Nikanorov et al.[77] The values of E and σ so obtained are consistent with those reported in the literature.[78] The density of silicon was taken as ρ(Si, 293.15 K, 0.1 MPa) = 2329.081 kg·m^{-3} based on the values reported by Bettin and Toth,[79] Fujii,[10] and Waseda and Fujii.[80,81] The variation of density with temperature and pressures ρ(Si, T, p) was obtained using

$$\rho(\mathrm{Si}, T, p - 0.1\ \mathrm{MPa}) = \rho(\mathrm{Si}, 293.15\ \mathrm{K}, 0.1\ \mathrm{MPa})\frac{[1 + \int_{298.15\ \mathrm{K}}^{T}\alpha(T)\,\mathrm{d}T]^3}{1 - \kappa_T(p/\mathrm{MPa} - 0.1)} \tag{17}$$

where α is the coefficient of linear thermal expansion, and κ_T is the isothermal compressibility. The ρ_s in eqs 13 and 14 is taken as ρ(Si, T, p) obtained from eq 17. We used the linear thermal expansion coefficient for cubic crystals that are isotropic[82] reported by Swenson[83] (and recommended by CODATA); Okaji[84] has, based on his measurements, provided an alternative and easier to use polynomial representation of the linear thermal expansion coefficient. The deformation of silicon crystals under hydrostatic pressure is isotropic because silicon is a cubic crystal,[82] and the isothermal compressibility (κ_T) of silicon can be determined from

$$\kappa_T = \frac{1}{\rho}\left(\frac{\partial \rho}{\partial p}\right)_T = 3(s_{11,T} + 2s_{12,T}) = \frac{3}{(c_{11,T} + 2c_{12,T})} \tag{18}$$

where $s_{11,T}$ and $s_{12,T}$ are the isothermal compliance and $c_{11,T}$ and $c_{12,T}$ isothermal stiffness that are determined from the

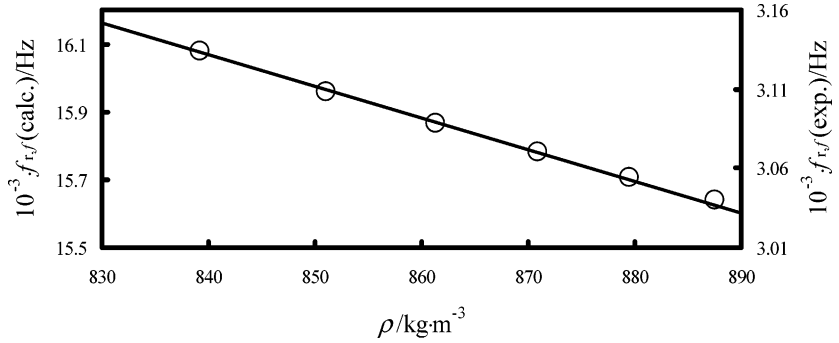

Figure 3. Frequency of the first eigenmode calculated from eq 13 $f_{r,f}$(calcd) with the mechanical properties provided by eqs 15 through 25 for the edge-supported plate immersed in methylbenzene at a temperature of 323.15 K and pressures between (0.1 and 68) MPa along with the experimentally determined frequency $f_{r,f}$(exp) as a function of density (ρ) determined from the correlation of Assael et al.[90] —, $f_{r,f}$(calcd) from eq 13 with left-hand ordinate axis; and ○, $f_{r,f}$(exp) with right-hand ordinate axis.

adiabatic compliance $s_{11,S}$ and $s_{12,S}$ given, in terms of the adiabatic stiffness, by

$$s_{11,S} = \frac{c_{11,S} + c_{12,S}}{(c_{11,S} - c_{12,S})(c_{11,S} + 2c_{12,S})} \quad (19)$$

and

$$s_{12,S} = \frac{-c_{12,S}}{(c_{11,S} - c_{12,S})(c_{11,S} + 2c_{12,S})} \quad (20)$$

The relationship between the adiabatic and isothermal compliances of

$$s_{11,S} - s_{11,T} = -\alpha^2 \frac{T}{\rho c_p} \quad (21)$$

and

$$s_{12,S} - s_{12,T} = -\alpha^2 \frac{T}{\rho c_p} \quad (22)$$

with the isothermal stiffness given by

$$c_{11,T} = \frac{s_{11,T} + s_{12,T}}{(s_{11,T} - s_{12,T})(s_{11,T} + 2s_{12,T})} \quad (23)$$

and

$$c_{12,T} = \frac{-s_{12,T}}{(s_{11,T} - s_{12,T})(s_{11,T} + 2s_{12,T})} \quad (24)$$

were also used in the analyses. In equations 21 and 22, ρ is the density of silicon and c_p is the massic heat capacity at constant pressure for silicon; both were obtained from ref 85. At a temperature of 295.65 K, $\kappa_T = 1.02 \cdot 10^{-11}$ Pa^{-1} (for octane the isothermal compressibility is $1.3 \cdot 10^{-9}$ Pa^{-1}) and a pressure change of 1 MPa results in a relative decrease in volume of $\Delta V/V \approx -1.04 \cdot 10^{-5}$. The differences between the adiabatic and isothermal compliances increase with increasing temperature. The pressure dependence of the isothermal compressibility of silicon crystals is obtained from

$$\kappa_T^{-1}(\partial \kappa_T/\partial p)_T = 2(3c_{111} + 6c_{112} + c_{123})/(c_{11} + 2c_{12})^2 \quad (25)$$

where the thermodynamic definitions of Brugger were used[86] with the third-order elastic constants c_{111}, c_{112}, and c_{123} reported by McSkimin and Andreatch[87,88] from speed of sound measurements. The third-order elastic constants reported by Philip and Breazeale[89] provide essentially the same values of $\kappa_T^{-1}(\partial \kappa_T/\partial p)_T$. When the effect of the third-order elastic constants is taken into account, the relative change in density from that obtained with the linear approximation of eq 17 is about $3.3 \cdot 10^{-5}$ at a temperature of 298 K and a pressure of 500 MPa, and its temperature dependence has been estimated to be negligible in our temperature range.[89] The linear thermal expansion coefficient and isothermal compressibility were also used to account for the variation of the plate dimensions a and d with temperature and pressure.

With the E, σ, and ρ_s determined from eqs 15 through 25 at a temperature of 323 K, eq 14 predicts $f_r(p = 0) = 57\,886$ Hz, which is about 4.9 times the measured value of 11 887 Hz. Equation 13 was used to estimate the resonance frequency when the MEMS was immersed in methylbenzene at a temperature of 323 K and pressures between (0.1 and 68) MPa. The density of methylbenzene required in the calculation was determined from the correlation of Assael et al.[90] The frequencies obtained from these calculations are shown as a solid line in Figure 3 with the scale defined by the left-hand ordinate along with the measured values (listed in Table 2) shown with open circles that refer to the scale defined by the right-hand ordinate. The measured frequencies are about a factor of 5.1 below the estimated values obtained from eq 13. The differences between the measured frequencies and those estimated from eqs 13 and 14 could arise from the approximations used to derive eq 13 and the assumption that the physical properties of the plate are equal to those of pure silicon.

The plate consists of 20 μm monocrystalline silicon onto which are deposited layers of aluminum, silicon nitride, silicon oxide, and aluminum nitride with fabrication processes (outlined in the Experimental Section) that require thermal cycling and chemical etching. It is therefore unreasonable to assume that the Young's modulus, Poisson's ratio, and density of the plate will be equal to those obtained for silicon; for silicon at $T =$ 323 K in a vacuum eqs 15 through 17 give $E \approx 129$ GPa, $\sigma \approx$ 0.265, and $\rho \approx 2\,328$ kg·m^{-3}. Indeed, Young's modulus for low-stress low-pressure chemical vapor deposited (LPCVD) silicon nitride has been reported to be (95 ± 10) GPa,[38] as determined from the resonance response of a cantilever plate, while that for LPCVD silicon dioxide has been reported as (61 ± 2) GPa.[91] The latter is about half that of silicon. A Poisson's ratio of (0.26 ± 0.01) has been reported for silicon dioxide.[91] The density of deposited silicon nitride has been reported as 2660 kg·m^{-3} by Santucci et al.[92] and 2865 kg·m^{-3} in ref 38 while Santucci et al.[92] gave values of 2210 kg·m^{-3} for thermally deposited silicon oxide and about 2400 kg·m^{-3} for CVD silicon oxide. Young's modulus of deposited aluminum can be up to 20 GPa[93] lower than that of the bulk material for

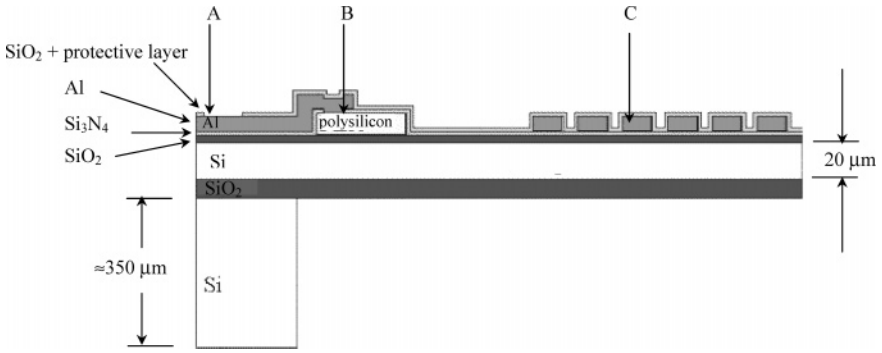

Figure 4. Schematic cross-section through the vibrating plate and supporting $350 \cdot 10^{-6}$ m thick silicon. Wire-bond pads A, Wheatstone bridge boron-doped polycrystalline silicon resistor B, and aluminum wire C that formed the coil.

which $E \approx 70$ GPa while aluminum nitride has $E \approx 300$ GPa.[94] Jianqiang et al. have reported that variations in the mechanical properties of the multiple layers that form cantilevers are an important factor in determining the resonance frequency of the cantilever when operated over a temperature range.[95] For the (1,0,0) crystallographic plane of silicon a cantilever plate, presumably operated at room temperature, has been used to obtain $E = (125.6 \pm 1.4)$ GPa,[39] which is 3.4 GPa below our value, and $\sigma = (0.2986 \pm 0.0017)$,[39] which is 0.034 (about 13 %) above our value.

In the absence of direct measurement of the E, σ, and ρ for each layer used to form the plate, two additional and unknown parameters (C_1 and C_2) that must be determined by calibration with a fluid of known density are included in eq 13 to give

$$\rho_f = \frac{C_2 E v_n^5 d^3}{24\{1-\sigma^2\}a^5(2\pi f_{r,f})^2} - \frac{C_1 \rho_s \, \mathrm{d} v_n}{2a} \qquad (26)$$

The parameters C_1 and C_2 also accommodate inadequate knowledge of the dimensions a and d. The calibration will be described in the Experimental Section.

There are other aspects of the MEMS design, fabrication, packaging, and operation that can also contribute, plausibly less than the physical properties of the plate, to the differences between the theoretical and observed resonance frequency. These effects include at least the following: (1) surface rugosity; (2) separation from stationary objects; (3) inertial response of the support; and (4) naive assumptions used to obtain eq 13. Each of these will be discussed briefly below.

Equation 13 (and thus the working eq 26) was derived assuming that the fluid−silicon interface is perfectly smooth. In practice, this means a surface rugosity much less than the viscous penetration depth; that is, it is optically flat. Our device (as shown in Figure 4) has surface undulations with dimensions of order $1 \cdot 10^{-6}$ m. When the surface is rough, the fluid motion caused by the oscillation is more complicated than for a smooth surface, and a range of additional mechanisms may occur that couple liquid motion and acoustic waves. Jain and Grimes[96] have considered (both experimentally and theoretically) the effect of surface roughness on liquid property measurements performed with mechanical oscillators. Their work suggests that, when the dimensions of the molecule are much less than those of the surface roughness, molecules are trapped on the surface and that they act as both an additional mass and a viscous load. Thus, it may be possible to alter the response of an oscillator immersed in a fluid by engineering a specific rugosity.[97] A simple but useful case might be when the rugosity traps largely immobilized fluid near the silicon surface, hence greatly enhancing the added mass (compared with a smooth surface) and thus rendering the device more sensitive to local fluid density. The dimensions of the molecules used in this work are of the order of 10^{-9} m while the surface undulations are of the order of 10^{-6} m.

The use of the plate's first mode forces the structure that holds the plate to recoil in response to the plate's motion. The plate's resonance frequency is thus coupled to the support. Increasing the mass of the plate's support reduces the mode coupling, which may result in a systematic error in density. In our case, the plate has a mass of about 0.1 mg while the packaged sensor has a mass of about 10 g excluding the Swagelock compression fitting. Finite element analyses suggest using either the $n = 2$ mode $\{f_r(p = 0) \approx 27.5$ kHz$\}$ (for which one side of the plate bends up while the other bends down) or the $n = 3$ mode $\{\{f_r(p = 0) \approx 70.3$ kHz$\}$ (where the center of the plate moves upward while the sides move downward) might reduce this potential source of error. Since these motions result in insignificant movement of the center of mass, the structure supporting the plate does not recoil so that the sensitivity of the tube's resonance frequency to the support is reduced. Preliminary investigations of the $n = 2$ and $n = 3$ modes provided promising results for density. Chang and Moldover[98] have considered this effect for the oscillating U-tube densimeter and recommended use of the $n = 3$ mode.

Chen et al.[99] and Nail et al.[100] investigated the variation in the resonance frequency of a cantilever with dimensions of order 1 mm immersed in a fluids as a function of separation of the cantilever from a stationary solid object. Both sets of measurements suggest that the resonance is affected when the oscillator is separated from the solid object by less than 1 mm. The results reported in refs 99 and 100 are consistent with both our preliminary measurements[101] and the calculations of Green and Sader[102] of the effect of separation of the plate from a stationary object. Our plate is separated from the nearest object by at least 1 mm.

Ultimately, the zeroth order or inviscid model must be modified to include viscous effects so that the working equations are coupled by describing the motion with the equation of continuity and the Navier−Stokes equations. Here we merely allude to a result that will be published in the future, where this will be done by modeling the flow using Stokeslets.[103] Such methods have previously been used to analyze the swimming motions of microscopic organisms such as flagella.[104−107] A numerical method for computing Stokes flows using Stokeslets has been described by Cortez.[108] In ref 108, a general case of Stokes flows driven by external forces was discussed. In principle, this method can be applied to any moving body interacting with fluid. However, we anticipate that the zeroth order model, which assumes density and viscosity can be

represented by independent equations, is probably not a significant source of error and will provide estimates of density and viscosity for the fluids studied over the density range (619 and 890) kg·m^{-3} and viscosities between (0.205 to 0.711) mPa·s because C_i with $i = 1$ and 2 are determined with a fluid of viscosity and density that includes these ranges. Manrique de Lara and Atkinson[109] and Manrique de Lara[111] have proposed an alternative model.

Models have been reported in the literature to obtain viscosity from the resonance frequency of a cantilever.[17,24−33,40,62−67] In this work, we have assumed that the fundamental bending mode of the plate (the flexural mode) is simple harmonic and that the plate is immersed in an unbounded Newtonian fluid of viscosity, η_f, and density, ρ_f, that affects the inertia (and thus to a certain extent the resonance frequency) and damping but not the elastic restoring force. The resonance quality factor, Q, is given by

$$Q^2 \propto (2\pi f_{r,f})^{-3}\eta_f\rho_f \tag{27}$$

at the resonance frequency (f_r). We note parenthetically that a viscoelastic fluid will alter the elastic restoring force. Including $Q\ \{= f_r/(2g)\}$ at $p = 0$, the working equation for fluid viscosity is given by

$$\eta_f = \frac{C_3}{\rho_f f_{r,f}^{\ 3}}\left\{\frac{2g_f}{f_{r,f}} - \frac{2g(p=0)}{f_r(p=0)}\right\}^2 \tag{28}$$

where $f_r(p = 0)$ is the resonance frequency in a vacuum; g_f is the resonance half-line width in the fluid, $g(p = 0)$ in a vacuum; ρ_f is the fluid density obtained from eq 13; and C_3 is a constant determined by calibration with a procedure described in the Experimental Section. The constant of proportionality in eq 28 includes the effective area, which is difficult to define but should be a constant for a given plate.

Apparatus and Experimental Procedures

MEMS Fabrication and Packaging. The design of the MEMS (shown in Figure 1) is similar to a device reported by Donzier et al.[54] The MEMS was processed on a 101.6 mm diameter silicon-on-insulator wafer (SOI) with crystallographic plane (1,0,0). It consists of a $20 \cdot 10^{-6}$ m monocrystalline silicon fusion bonded to a silicon oxide layer (about $0.5 \cdot 10^{-6}$ m thick and called buried oxide or BOX) that isolates the upper layer from the monocrystalline silicon wafer below that has a thickness of about $350 \cdot 10^{-6}$ m. The use of the SOI wafer as the starting material simplifies the deep reactive ion etch used in the micro-machining and precisely defines the plate's thickness prior to layer deposition. About 600 transducers, of the type shown in Figure 1, were processed on one 101.6 mm diameter wafer. The processes required to fabricate the transducer include photolithography (as used in integrated circuit fabrication) and deep reactive ion etching for the micro-machining. Photolithography uses ultraviolet (UV) sensitive material (photoresist) and masks that define shapes, and when this combination is exposed to UV, the resulting patterned surface is chemically etched to remove the unwanted materials deposited onto the wafer to form particular elements, for example, resistors. To actuate and sense the plate's motion as well as interconnect with the external electronics five boron-doped polycrystalline silicon resistors and aluminum wire (both shown in the cross-sectional view of Figure 4 as well as the top view in Figure 1) were deposited onto the $20 \cdot 10^{-6}$ m monocrystalline silicon. Four of these resistors (shown in Figures 1, 2, and 4) were located close to where the $20 \cdot 10^{-6}$ m thick plate meets the $350 \cdot 10^{-6}$ m thick underlying wafer: two were located parallel and two were perpendicular to the supporting edge. These four resistors formed a strain gauge that was configured as a Wheatstone bridge that was used, as described below, to determine the motion and thus resonance frequency of the plate. We required the resistance of these four resistors to be stable relative to each other over the time required to determine the resonance frequency; an accurate absolute measurement of the strain is not required in this transducer as it is for other sensors such as those used to measure pressure. The optimal location of the strain gauge resistors was determined by finite element analysis. The fifth resistor could be (but was not in this work) used as temperature detector. Aluminum was deposited and photolithography performed to obtain wire that provided an excitation coil as well as electrical connections between the wire-bond pads, the bridge, the thermometer resistors, and the coil used to excite motion.

The complete fabrication process, which is similar in many respects to that described by Bourouina et al.,[110] will be presented elsewhere and only an outline of the procedures is provided here as they are in ref 111. The MEMS were fabricated by École Supérieure d'Ingénieurs en Électrotechnique et Électronique (ESIEE). Atop the $20 \cdot 10^{-6}$ m wafer was deposited about $0.3 \cdot 10^{-6}$ m of silicon dioxide onto which was deposited about $0.4 \cdot 10^{-6}$ m of polycrystalline silicon that was then annealed. The polycrystalline silicon was then doped, by ion implantation, with boron to adjust the resistance and gauge factor. The polycrystalline silicon was patterned by photolithography, and the polycrystalline silicon not covered with photoresist was subsequently removed by dry reactive ion etching (RIE). This process formed boron-doped polycrystalline silicon resistors each with a resistance of about 800 Ω at a temperature of 297 K. Four of these resistors formed a Wheatstone bridge strain gauge, while the fifth resistor was a temperature detector that had a resistance of about 600 Ω at a temperature of 298 K. Silicon nitride, with stoichiometry similar to Si_3N_4, of thickness about $0.1 \cdot 10^{-6}$ m was deposited atop the surface coated in etched polysilicon by low-pressure chemical vapor deposition (LPCVD) to form a chemically inert insulating layer. A $1 \cdot 10^{-6}$ m thick aluminum layer was deposited by sputtering on to the silicon nitride that, after photolithography, formed metal lines (shown in Figures 1, 2, and 4) defining both a coil and electrical contacts between the coil and resistors to the wire-bond pads. The aluminum wire that formed the coil has (as shown schematically in Figure 4) a rectangular cross-section with a line width of about $15 \cdot 10^{-6}$ m and total length of about 6 cm. The wire had a resistance of about 300 Ω at a temperature of $T = 298$ K. Each turn of the coil was separated from the adjacent wire by a distance of about $5 \cdot 10^{-6}$ m. To protect the transducers from the environment in which they would be immersed, two additional layers were deposited atop the wafer. First, a layer of silicon dioxide about $0.5 \cdot 10^{-6}$ m thick was deposited that was then followed by a layer of protective material that was about $0.6 \cdot 10^{-6}$ m thick. These additional layers underwent photolithography at the wire bond pads to expose the aluminum so that electrical contacts could be made. Deep reactive ion etching (DRIE) was then used on the top-face to remove the additional layers and the $20 \cdot 10^{-6}$ m thick silicon in a groove around three sides of the plate.[112] The BOX acted as an etch stop. A second DRIE micro-machining step was performed from the back of the chip to remove the underlying 0.350 mm of silicon with the BOX acting as a etch stop that was also removed with further micro-machining. The result edge supported plate was about 1.45 mm

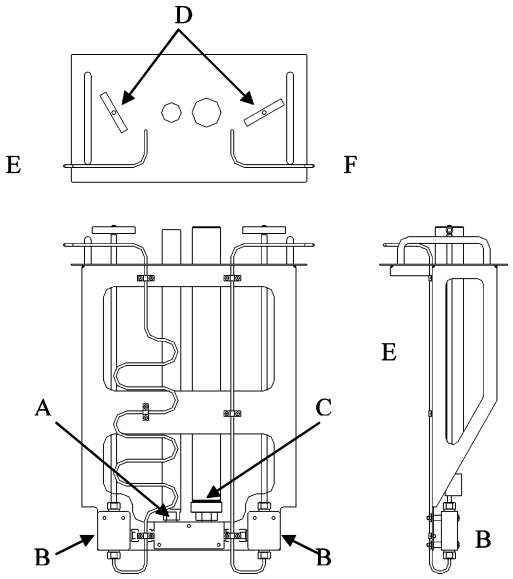

Figure 5. Schematic of the assembly that holds the MEMS and pressure gauge and is immersed in a stirred fluid bath. Bottom left: pressure gauge A, MEMS C, and valves B. Top: valve handles D, inlet tubes E, and outlet tubes F. Bottom right: side view showing the valve B and inlet tube E.

long and 1.8 mm wide with a thickness, which varied over the surface area, from (21.6 to 23) · 10^{-6} m with an estimated average thickness over the plate of ≈ 22.25 · 10^{-6} m. The individual devices on a wafer were separated from each other with a process known as dicing.

Each MEMS was wire-bonded (ultrasonically) to one end of a printed circuit board (PCB) fabricated from polyimide that was about 50 mm long. The other end of the PCB had solder pads through which external electronics could be connected to the active elements of the MEMS. The wire bond pads (shown at right of Figure 1 and left of Figure 4) and the PCB were sealed, with the moving element of the MEMS exposed at one end and the solder pads of the PCB exposed at the other end, within a 3.175 mm o.d. stainless steel, type 316, tube with an adhesive. Prior to inserting the PCB into the tube, a Swagelock fitting was compressed onto the tube about 25 mm from the end from which the MEMS protruded. This arrangement, which acted as a pressure tight electrical feedthrough, was solely intended to provide a means of evaluating the MEMS immersed in fluids at temperatures and pressures above ambient. However, when the adhesive was used as a pressure seal the upper operating temperature was limited to temperatures below 448 K and the upper operating pressure to less than 130 MPa. The theoretical upper operating temperature of the MEMS, without packaging, is limited to about 490 K by the boron doped polycrystalline silicon resistors.

Evaluation Apparatus. The apparatus used to thermostat and expose the packaged MEMS to fluids at pressure is shown in Figure 5. The packaged MEMS A, shown in Figure 5, was inserted into the top of a block that also contained a port for the pressure C, shown in Figure 5, and at each end of the block, there were tubes for fluid to be flushed through the mounting block. The volume of the system between valves B of Figure 5 was about 2 cm^3. These valves were sealed during the time required for data acquisition. At the other end of each of these tubes was located another valve not shown in Figure 5. The PCB protruding from the end furthest from the plate, to which interconnecting wires were soldered, was protected from the thermostat fluid by a tube A, shown in Figure 5, that was sealed with an O-ring. A bobbin, not shown in Figure 5, about 40 mm long and manufactured from aluminum, contained about 700 turns of polyimide-coated copper wire of diameter 0.3 mm, and it was mounted outside the protective tube A so that the MEMS plate was in the center of the bobbin. A dc current was passed through the coil to form an electromagnet that provided the magnetic flux (B; shown in Figure 2) perpendicular to the tip of the vibrating plate. When about 1 A (at a voltage of about 25 V dc) was applied to the coil at $T = 298$ K a flux of about 0.1 T, determined with a magnetic flux meter, was generated within the center of the bobbin about the location of the plate; because of the relatively high heat capacity of the rapidly stirred bath fluid and the thermal conductivity of the metallic enclosure, the ≈ 25 W dissipated in the electromagnet did not cause a significant local temperature rise. The aluminum coil on the plate was driven with a frequency synthesizer (Agilent model 33120A) that was phase-locked to a global positioning satellite stabilized 10 MHz time-base (Symmetricon model 58503B) to give a relative resolution and accuracy in frequency of ≈ 10^{-11} and < 10^{-11}, respectively. As $p \rightarrow 0$ the synthesizer was set to provide a signal amplitude of 0.15 V ac peak-to-peak (the minimum required to attain lock with the detector) while at $p > 0$ the voltage was increased to be about 1 V ac peak-to-peak at the highest densities studied; for a given temperature, this approach maintained about the same signal-to-noise ratio over the whole density range and provided a resonance frequency that was independent of the drive voltage. When the ac current ($i \approx 1$ mA in Figure 2) flowed through the coil in the presence of the magnetic field the plate moved at the frequency of the current as illustrated schematically in Figure 2. The Wheatstone bridge, located near the plate support, was supplied with 0.5 V dc, and when the plate is forced to vibrate, the bending motion results in a variation in the resistance of two of the bridge resistors so that an ac out-of-balance voltage is generated proportional to the displacement velocity. The complex ac voltage generated by the plate's motion is detected with a lock-in amplifier (SRS model 850), set at a time-constant of 0.3 s, relative to the complex voltage sent to the coil; the voltage was determined by a differential measurement between the two lock-in input channels. When the MEMS was immersed in a fluid the $f_r(T, p)$ and $Q(T, p)$ {$= f_r/(2g)$} were considered determined after three consecutive measurements of T, p, and f met the following criteria: $\Delta T/T < 10^{-5}$, $\Delta p/p < 10^{-4}$, and $\Delta f/f < 10^{-5}$.

The resonance frequency (f_r) and line half-width (g) of the well-resolved singlet mode (1,0) {the $f_r(2,0) \approx 27.5$ kHz at $p = 0$} were obtained from measurements of the in-phase $u(f)$ and quadrature $v(f)$ voltages at 11 discrete frequencies (f) from ≈ (f_r − g) in steps of $g/5$ to ≈ ($f_r + g$) and then back to ≈ ($f_r - g$) close to f_r. The resonance scan was reversed from ≈ ($f_r + g$) to ≈ (f_r − g) to ensure that temperature drifts, which would have lead to a serious error in the measurement of g, had not occurred during the course of the measurements. After each frequency step the system waited a time, which is a multiple of the slowest relaxation time of the measurement, prior to measuring the complex voltage. In our case, this time was determined by the post detection lock-in time constant. The f_r and g were obtained from the measured $u(f)$ and $v(f)$ by assuming that the resonance took the form:

$$u + iv = -\frac{i\boldsymbol{D}f}{[(f_r + ig)^2 - f^2]} + \boldsymbol{E} \qquad (29)$$

In eq 29, $\boldsymbol{D}$ is a complex amplitude proportional to the source strength and phase shifts and $\boldsymbol{E}$ is the leading complex term in a Taylor series for f near f_r. The $\boldsymbol{E}$ accounts for the background

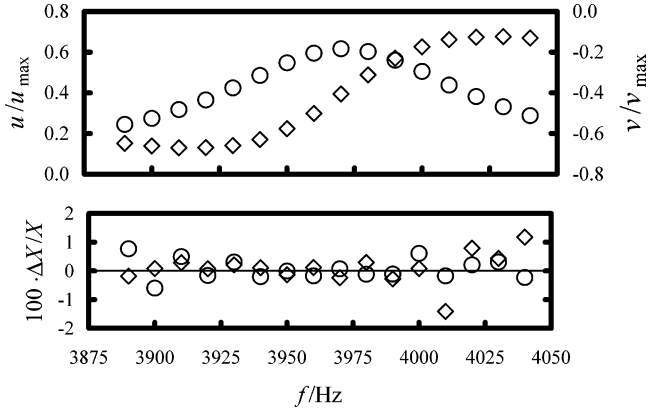

Figure 6. Top: Measured in-phase u and quadrature voltage v as a function of frequency over the (1,0) fundamental mode of the flexural plate in methylbenzene at a temperature of 323.212 K and pressure of 5.4723 MPa where according to Assael et al.[90] the density is 843.9 kg·m^{-3} and the viscosity is 0.4401 mPa·s. The complex voltage was obtained from the Wheatstone bridge relative to the complex voltage sent to the coil as a ratio of the maximum detectable voltage of the lock-in at a sensitivity of 5 mV. Bottom: relative differences $\Delta X/X = \{X(\text{expt}) - X(\text{calcd})\}/X_{max}$ where $X = u$ or v of the measured X(expt) minus the calculated voltages X(calcd) from eq 29[113] with the following fitted parameters: $f_r + ig = (3970.7231 + i55.7176)$ Hz, $\boldsymbol{D} = (60.9400 + i0.8344)$, $\boldsymbol{E} = -(0.3964 + i0.0695)$. X_{max} is the maximum u or v. The data were taken at intervals of 10 Hz from the lowest to the highest frequency and then back to the lowest. Drifts in the temperature of the apparatus or the lock-in would be detected from variations in the measured values. For the sake of clarity one-fifth of the measurements are shown. ○, u; ◇, v.

signal arising from tails of resonances other than the one under study. The parameters appearing in eq 29 were determined using a nonlinear regression algorithm developed by Mehl[113] with initial estimates of the adjustable parameters, required for the nonlinear regression, obtained from a Lorentzian fit to the measurements. The uncertainty in a determination of resonance frequency depends on the Q of the resonance. For $Q \approx 10$ our measurements and eq 29 returned a standard deviation in resonance frequency $\sigma(f_r) < 0.1$ Hz. Inclusion of the frequency dependent background in eq 29 was never justified based on a significant reduction in χ^2 of the fit.

Equation 29 was originally applied to the determination of the complex frequency of acoustic modes within a spherical cavity. To demonstrate that eq 29 is suitable for the analysis of the response of the MEMS plate, we show in the top of Figure 6 the measured complex voltage $(u + iv)$ at 60 frequencies spanning the range $\pm 2g$ of f_r. In most cases, as shown in the lower plot of Figure 6, the fit to the measured voltages provided by eq 29 had a precision of better than $\pm$ 0.3 % of the maximum voltage. The deviations from the fit did not exceed the noise. It therefore follows that f_r is determined with a precision of about $\pm$ 0.3 % of g that is fractionally about $6 \cdot 10^{-7}$ in a vacuum and $5 \cdot 10^{-5}$ in a liquid such as methylbenzene. To this extent this resonator does indeed behave as predicted by eq 29. For the sake of clarity, only one-fifth of the measurements are shown in Figure 6.

The MEMS and pressure gauge held within the evaluation apparatus were suspended in and thermostated by a stirred fluid bath (Hart Scientific model 6022) containing a poly(dimethylsiloxane) polymer $(CH_3)_3SiO[SiO(CH_3)_2]_nSi(CH_3)_3$ (Dow Corning 200-20 with CAS Registry No. 63-148-62-9). This thermostat had both a vertical and horizontal temperature stability of $< \pm$ 0.003 K when operated in the temperature range (323 to 448) K. The temperature of the bath fluid was determined on the International Temperature Scale of 1990 (ITS-90) using a long-stem platinum resistance thermometer (Isotech model 909B), with the center of the sensing element located in the same horizontal plane as the plate, and an ac ratio-transformer bridge (ASL F300 with a nominal 25 Ω Wilkins standard resistor) that gave a resolution of $\pm$ 1 mK and an accuracy, at each temperature, specified by ITS-90. During the time required to measure the resonance frequency, the temperature of the bath fluid varied, in the worst case, by about $\delta T = 3$ mK. In the remainder of the analysis, we assume the uncertainty in the temperature of the fluid to which the MEMS is exposed is equal the variations in the bath fluid temperature. However, the mounting block presumably damped the bath fluid temperature fluctuations, and it is reasonable to assume that this estimate represents an upper bound for the variations of the temperature of the fluid in which the MEMS was immersed. Nevertheless, the $\delta T = 3$ mK results in an almost negligible uncertainty in density of $\delta\rho < 0.003$ kg·m^{-3} (about 0.0004 %) because for the fluids investigated over our temperature and pressure range $|(\partial\rho/\partial T)_p| < 1$ kg·m^{-3}·K^{-1}. This $\delta T \approx 0.003$ K also gives rise to an insignificant (<0.003 %) variation in viscosity on the reasonable assumption that $|(\partial\eta/\partial T)_p| < 7 \cdot 10^{-6}$ Pa·s·K^{-1}. We conclude that temperature variations result in a negligible uncertainty in our measured density and viscosity.

Pressures greater than 0.1 MPa were measured using a resonant quartz transducer (Quartzdyne model QHB009-16-200 serial number 157 972 with a maximum operating pressure of 110 MPa and maximum operating temperature of 473 K) with an accuracy cited by the manufacturer of about 0.02 % of full scale. When the pressure transducer was calibrated against an oil-lubricated dead-weight gauge it was found to have an uncertainty of δp/MPa = $\pm$ {0.0001·(p/MPa) + 0.022}, where the quantity 0.022 MPa is about 0.02 % of the full-scale pressure of 110 MPa. The pressure gauge was immersed in the stirred fluid bath and mounted at location C shown in Figure 5. In the temperature and pressure range investigated the $\delta p < 0.029$ MPa and, when combined, in the worst case, with $(\partial\rho(C_8H_{18}, 423 \text{ K}, 7 \text{ MPa})/\partial p)_T \approx 2$ kg·m^{-3}·MPa^{-1} corresponds to a potential uncertainty in density of 0.05 kg·m^{-3} (or about 0.007 %). For viscosity, in the worst case, $(\partial\eta/\partial p)_T \approx 5$ mPa·s·MPa^{-1} and the $\delta p \approx 0.029$ MPa corresponds to an uncertainty in viscosity of < 0.02 %. The density, viscosity, and derivatives with respect to pressure and temperature were determined from literature values described in the Results and Discussion section below. Pressures were generated in the system with an ISCO model 100 DX positive displacement pump with an upper operating pressure of about 68 MPa, which limited the upper operating pressure of the MEMS. Pressures of about 0.1 MPa were measured using a resonating quartz barometer (Paroscientific 740-16B with a maximum operating pressure of 0.11 MPa) with an accuracy cited by the supplier of 0.008 % of full-scale (about 8.8 Pa).

Prior to measurements with each fluid, the apparatus was evacuated, with a turbo-molecular pump, to a pressure (as indicated by an ionization gauge located near the pump) of less than 10^{-2} Pa for at least 24 h. The pressure within the apparatus where the MEMS is located could have been considerably higher owing to the low pumping impedance of the high-pressure tube that is about 1 m long and has 0.8 mm i.d. Between measurements with each fluid, the apparatus temperature was set to a temperature of 373 K and evacuated for about 12 h. The apparatus was cooled to $T = 323$ K and flushed three times with the fluid to be investigated.

At $T = 423$ K our measurements were affected by a lower signal-to-noise ratio. Plausible explanations for this decrease might arise from a decreased magnetic flux and a greater thermal

Table 1. Resonance Frequency f_r, the Resonance Line Half-Width g, and the Quality Factor Q, $\{= f_r/(2g)\}$ at Temperature T, and a Pressure of about $5 \cdot 10^{-3}$ Pa Determined with an Ionization Gauge Separated from the MEMS by about a 1 m Length of 0.8 mm i.d. Tube[a]

T/K	$f_r(p \rightarrow 0)$/Hz	$g(p \rightarrow 0)$/Hz	Q
323.151[b] ± 0.003	11886.5943 ± 0.0080	2.6614 ± 0.0080	2233.147
348.144 ± 0.003	11887.313 ± 0.020	2.436 ± 0.020	2439.624
373.123 ± 0.003	11865.2865 ± 0.0059	2.7023 ± 0.0059	2195.405
373.111 ± 0.003	11876.164 ± 0.011	2.757 ± 0.011	2154.133
423.091 ± 0.003	11838.078 ± 0.082	7.646 ± 0.082	774.186

[a] The uncertainties given in f_r and g are one standard uncertainty as determined from the fit of the measured in-phase and quadrature voltage to eq 29. [b] Used to determine C_1 and C_2.

noise of the Wheatstone bridge. However, no experiments were performed to identify and correct the observation. This reduction in signal-to-noise results in resonance frequencies and half resonance line-widths with uncertainties greater by a factor of between (5 and 10) over those obtained at lower temperatures. These greater errors propagate to increase the errors in density and particularly viscosity.

Materials. The octane used was supplied by Aldrich with a mass fraction purity greater than 0.99 as anhydrous and containing mass fractions less than $< 2 \cdot 10^{-5}$ of water and $< 3 \cdot 10^{-4}$ of an unspecified solid residue after evaporation. Methylbenzene was supplied with a mass fraction purity greater than 0.998 and contained a mass fraction of water less than $3 \cdot 10^{-4}$. Chemical compositional analyses were performed neither before nor after the measurements, and we have assumed that there were no variations in chemical composition from those cited by the supplier. The samples were degassed by vacuum sublimation and dried over a 0.4 nm molecular sieve for about 24 h. Prior to use the molecular sieve was heated for at least 48 h to a temperature > 500 K while maintaining the pressure at < 1 mPa with a turbo-molecular pumping station. Although no measurements were performed to identify the impurities in the samples it is plausible that there were hydrocarbons of similar normal boiling temperature $\{T(\mathrm{lg}, p = 0.1\ \mathrm{MPa})\}$ to those of the major constituent. A mole fraction $x \approx 0.01$ of those chemicals would introduce an uncertainty of < 0.1 % in both the measured density and viscosity.

Calibration. The resonance frequency (f_r) and line half-width (g) were measured at a temperature of 323 K in a vacuum (listed in Table 1) and when the plate was immersed in methylbenzene (listed in Table 2) at pressures below 68 MPa. The resonance frequencies were combined with both the elastic properties, described above, and the density was estimated from the correlation reported by Assael et al.[90] (determined from our measurements of temperature and pressure) to obtain values for C_1 and C_2 in eq 26 under the constraint the resonance frequency measured in a vacuum and listed in Table 1 must be reproduced by

$$f_r(p = 0) = (2\pi)^{-1}\left[\frac{C_2 E v_n{}^4 d^2}{12\{1 - \sigma^2\}a^4 \rho_s C_1}\right]^{1/2} \qquad (30)$$

with the same C_1 and C_2. The parameter C_3 in eq 28 was determined by regression on the resonance frequencies and line half-widths combined with the density of silicon and the density and viscosity obtained from ref 90. The values of the C_i values with $i = 1$, 2, and 3 so determined are listed in Table 3. The densities of stoichiometric monocrystalline materials atop the silicon are greater than that of pure silicon, and thus one might expect C_1 to be greater than unity; however, the deposited

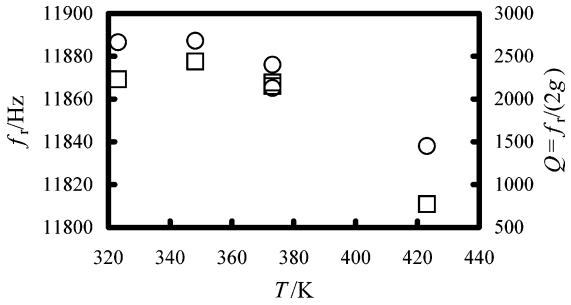

Figure 7. Resonance frequency f_r and quality factor Q of the (1,0) fundamental mode of the edge-supported plate at a pressure of about $5 \cdot 10^{-3}$ Pa determined by an ionization gauge separated from the MEMS by about a 1 m length of 0.8 mm i.d. ○, f_r; □, Q.

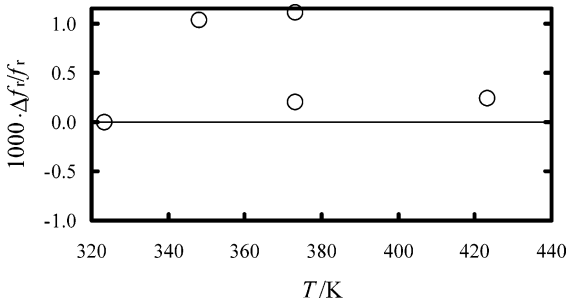

Figure 8. Relative fractional difference $\Delta f_r/f_r = \{f_r(\mathrm{expt}) - f_r(\mathrm{calcd})\}/f_r(\mathrm{calcd})$ of the experimentally determined resonance frequency $f_r(\mathrm{expt})$ from the calculated resonance frequency $f_r(\mathrm{calcd})$ determined from eq 14 with the calibration coefficients C_1 and C_2 of Table 3 and the temperature-dependent elastic properties and density of silicon described in the text as a function of temperature. The pressure was about $5 \cdot 10^{-3}$ Pa as determined by an ionization gauge separated from the MEMS by about a 1 m length of 0.8 mm i.d. tube. ○, f_r.

materials are probably neither stoichiometric nor monocrystalline. This might explain why C_1 determined from the measurements is about 11 % below unity. The elastic properties of the additional layers are less than that of silicon and presumably this (along with the process used to deposit the layers) drastically reduces the effective Young's modulus (E) and thus reduced C_2 from unity. The first term of eq 26 contributes between (899.5 to 950.6) kg·m^{-3} to the measured density that arises mostly from variation in the resonance frequency while the second term varies by 0.04 kg·m^{-3} from −(62.53 to 62.49) kg·m^{-3}, a variation that arises solely from the pressure dependence of both the density and elastic properties of silicon.

The measured resonance frequencies (f_r) and quality factors (Q) obtained in a vacuum as a function of temperatures in the range (323 to 423) K are shown in Figure 7. As expected, both f_r and Q decrease with increasing temperature. The resonance frequencies as $p \rightarrow 0$ are shown in Figure 8 as fractional deviations from the values obtained from eq 30 with C_1 and C_2 of Table 3 that never exceed 0.11 %. However, the values of $Q(p \rightarrow 0)$ listed in Table 1 are significantly lower (at least a factor of 10) than anticipated from the measurements reported for cantilevers by Blom et al.[114] and Yasumura et al.[115] and from naive calculations for our plate. At a pressure of about 1 Pa the Q values reported by Bruschi et al.[116] are of the same order of magnitude as our observations listed in Table 1.

The densities determined using eq 26 at a temperature of 323 K with the C_1 and C_2 listed in Table 3 are shown in Figure 9 as relative deviations from the values obtained from the correlation of Assael et al.[90] and all lie within ± 0.1 %. The correlation of Assael et al.[90] has an estimated expanded ($k = 2$) uncertainty in density of about 0.1 % that is shown in Figure 9 with a broken line. Our results deviate from ref 90 within the

Table 2. Density ρ, and Viscosity η, of Fluid i, Determined from the MEMS Resonance Frequency $f_{r,f}$, and the Resonance Half Line-Width g_f as a Function of Mean Pressure $\langle p \rangle$ at the Given Mean Temperatures $\langle T \rangle$[a]

i	$<T>$/K	$\langle p \rangle$/MPa	$f_{r,f}$/Hz	g_f/Hz	ρ/kg·m^{-3}	$\eta/10^{-6}$ Pa·s
methylbenzene	323.151[b] ± 0.003	0.100 ± 0.022	3134.271 ± 0.037	54.256 ± 0.037	837.0 ± 1.7	421 ± 10
		13.940 ± 0.023	3108.988 ± 0.051	57.256 ± 0.051	850.7 ± 1.7	482 ± 12
		27.338 ± 0.025	3088.675 ± 0.046	59.128 ± 0.046	861.7 ± 1.7	524 ± 13
		41.055 ± 0.026	3070.661 ± 0.043	61.104 ± 0.043	871.5 ± 1.7	571 ± 14
		54.593 ± 0.027	3054.941 ± 0.063	62.898 ± 0.063	880.1 ± 1.8	615 ± 15
		68.135 ± 0.029	3040.4094 ± 0.0080	64.682 ± 0.008	888.1 ± 1.8	660 ± 16
methylbenzene	373.111 ± 0.003	13.270 ± 0.023	3179.396 ± 0.022	46.1629 ± 0.022	807.3 ± 1.6	292.4 ± 7.1
		26.975 ± 0.025	3150.19 ± 0.11	49.0257 ± 0.11	822.5 ± 1.6	339.8 ± 8.8
		40.789 ± 0.026	3127.773 ± 0.067	50.5215 ± 0.067	834.2 ± 1.7	369.1 ± 9.2
		54.631 ± 0.027	3107.36 ± 0.13	53.2504 ± 0.13	845.0 ± 1.7	419 ± 11
		68.196 ± 0.029	3091.430 ± 0.028	53.8692 ± 0.028	853.4 ± 1.7	436 ± 11
octane	323.151 ± 0.003	0.100 ± 0.022	3459.191 ± 0.043	59.943 ± 0.043	676.0 ± 1.4	389.2 ± 9.5
		10.096 ± 0.023	3430.717 ± 0.049	62.901 ± 0.049	687.7 ± 1.4	440 ± 11
		20.701 ± 0.024	3405.52 ± 0.11	65.95 ± 0.11	698.1 ± 1.4	495 ± 12
		30.654 ± 0.025	3385.235 ± 0.057	67.644 ± 0.057	706.7 ± 1.4	530 ± 13
		41.050 ± 0.026	3366.477 ± 0.080	69.920 ± 0.080	714.6 ± 1.4	576 ± 14
		54.543 ± 0.027	3344.647 ± 0.068	72.521 ± 0.068	723.9 ± 1.4	633 ± 16
		68.036 ± 0.029	3325.290 ± 0.077	75.224 ± 0.077	732.2 ± 1.5	693 ± 17
octane	348.144 ± 0.003	0.100 ± 0.022	3507.68 ± 0.16	53.77 ± 0.16	654.3 ± 1.3	301.1 ± 8.1
		7.551 ± 0.023	3481.27 ± 0.13	55.96 ± 0.13	664.7 ± 1.3	333.8 ± 8.7
		13.680 ± 0.023	3462.78 ± 0.09	56.946 ± 0.092	672.2 ± 1.3	351.3 ± 8.8
		20.500 ± 0.024	3444.94 ± 0.17	58.57 ± 0.17	679.4 ± 1.4	378 ± 10
		27.466 ± 0.025	3428.47 ± 0.06	59.895 ± 0.065	686.1 ± 1.4	400.8 ± 9.9
		27.469 ± 0.025	3428.56 ± 0.12	59.85 ± 0.12	686.1 ± 1.4	400 ± 10
		34.314 ± 0.025	3416.76 ± 0.04	61.265 ± 0.037	690.8 ± 1.4	424 ± 10
		34.305 ± 0.025	3413.78 ± 0.03	61.197 ± 0.033	692.1 ± 1.4	424 ± 10
		41.227 ± 0.026	3400.08 ± 0.04	62.595 ± 0.041	697.8 ± 1.4	449 ± 11
		41.226 ± 0.026	3399.95 ± 0.04	62.563 ± 0.037	697.9 ± 1.4	449 ± 11
		48.070 ± 0.027	3387.30 ± 0.07	63.719 ± 0.070	703.1 ± 1.4	471 ± 12
		55.004 ± 0.028	3375.32 ± 0.05	65.188 ± 0.055	708.1 ± 1.4	499 ± 12
		55.000 ± 0.028	3375.25 ± 0.06	65.159 ± 0.058	708.2 ± 1.4	498 ± 12
		61.994 ± 0.028	3364.30 ± 0.21	67.07 ± 0.21	712.8 ± 1.4	533 ± 15
		61.992 ± 0.028	3361.17 ± 0.24	66.26 ± 0.24	714.2 ± 1.4	522 ± 15
octane	373.120 ± 0.003	6.723 ± 0.023	3527.003 ± 0.032	51.893 ± 0.032	644.7 ± 1.3	275.7 ± 6.7
		6.724 ± 0.023	3527.059 ± 0.025	51.902 ± 0.025	644.6 ± 1.3	275.8 ± 6.7
		20.592 ± 0.024	3480.471 ± 0.070	54.826 ± 0.070	662.9 ± 1.3	320.5 ± 8.0
		20.599 ± 0.024	3480.347 ± 0.054	54.920 ± 0.054	662.9 ± 1.3	321.7 ± 7.9
		27.397 ± 0.025	3461.93 ± 0.13	56.24 ± 0.13	670.3 ± 1.3	342.9 ± 9.0
		27.402 ± 0.025	3461.72 ± 0.13	56.24 ± 0.13	670.4 ± 1.3	342.9 ± 8.9
		34.317 ± 0.025	3444.826 ± 0.032	57.554 ± 0.032	677.1 ± 1.4	364.6 ± 8.9
		34.324 ± 0.025	3444.786 ± 0.039	57.574 ± 0.039	677.2 ± 1.4	364.9 ± 8.9
		41.184 ± 0.026	3429.08 ± 0.16	58.42 ± 0.16	683.5 ± 1.4	381 ± 10
		41.207 ± 0.026	3428.95 ± 0.16	58.36 ± 0.16	683.6 ± 1.4	380 ± 10
		41.221 ± 0.026	3428.90 ± 0.14	58.65 ± 0.14	683.6 ± 1.4	384 ± 10
		48.024 ± 0.027	3415.264 ± 0.029	60.123 ± 0.029	689.2 ± 1.4	409 ± 10
		48.032 ± 0.027	3415.285 ± 0.031	60.172 ± 0.031	689.1 ± 1.4	409 ± 10
		54.853 ± 0.027	3402.088 ± 0.069	61.484 ± 0.069	694.6 ± 1.4	433 ± 11
		54.866 ± 0.027	3401.995 ± 0.048	61.465 ± 0.048	694.6 ± 1.4	432 ± 11
		61.686 ± 0.028	3389.411 ± 0.035	62.115 ± 0.035	699.8 ± 1.4	447 ± 11
		61.704 ± 0.028	3389.362 ± 0.036	62.297 ± 0.036	699.8 ± 1.4	449 ± 11
octane	423.090 ± 0.003	14.725 ± 0.023	3580.49 ± 0.66	49.72 ± 0.66	620.5 ± 1.3	229 ± 13
		27.159 ± 0.025	3531.67 ± 0.72	51.07 ± 0.72	638.8 ± 1.3	252 ± 16
		40.831 ± 0.026	3488.50 ± 0.83	53.37 ± 0.83	655.5 ± 1.4	287 ± 19
		54.591 ± 0.027	3454.60 ± 0.79	57.44 ± 0.79	668.8 ± 1.4	344 ± 21
		68.420 ± 0.029	3434.9 ± 1.1	57.6 ± 1.1	676.4 ± 1.5	352 ± 29

[a] Pressures and temperatures reported are an average of two measurements (one obtained before the other after acquiring the complex voltages as a function of frequency). The standard deviation of the mean temperature was less than 1 mK. The standard uncertainties in T and p are reported. The values of $f_{r,f}$ and g_f were determined from an analysis of the complex voltages obtained with both increasing and decreasing frequency. The uncertainties in $f_{r,f}$ and g_f are one standard deviation as determined from the fit of the measured in-phase and quadrature voltages to eq 29. The combined expanded ($k = 2$) uncertainties in density and viscosity include those arising from the complex resonance, temperature, pressure, and calibration combined in-quadrature. [b] Used to determine C_1, C_2, and C_3.

Table 3. Values of C_i with $i = 1$, 2, and 3 of Equations 13, 14, and 28 Obtained from Measurements with Methylbenzene at a Temperature of 323.15 K (listed in Table 2) at Pressures between (0.1 and 68) MPa along with the f (323 K, $p \rightarrow 0$) of Table 1

T/K	C_1	C_2	C_3/kg^2·m^{-4}·s^{-5}
323.15	0.8915035	$3.759206 \cdot 10^{-2}$	$9.298190195 \cdot 10^{12}$

estimated expanded uncertainty except at $p = 0.1$ MPa where our measurement lies −0.25 % below ref 90; in this range the deviations increase with increasing pressure. Based on the measurements performed, we have been unable to identify the source of these differences. Nevertheless, we take the average of the absolute differences of ± 0.1 % as a measure of the anticipated precision in the measurements of density with this instrument. The densities reported in refs 126−133 and 136−139 are also shown in Figure 9 relative to ref 90 and all deviate between −0.25 % and +0.2 %. In Figure 9, the measurements reported by Pöhler and Kiran[141] are systematically low by 0.4 %.

The viscosities determined at $T = 323$ K from eq 28 with the measured Q combined with C_3 (listed in Table 3) and the

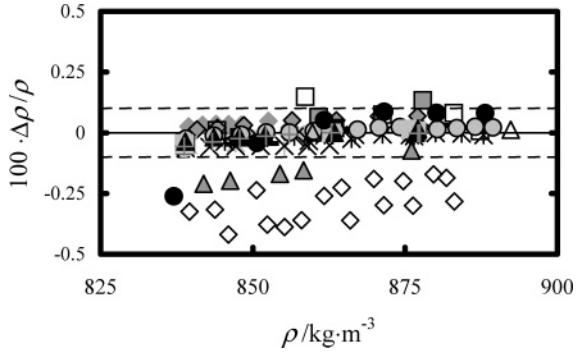

Figure 9. Fractional deviations $\Delta\rho = \rho(\text{expt}) - \rho(\text{calcd})$ of the experimental densities ρ(expt) of methylbenzene at $T \approx 323.15$ K from values ρ(calcd) obtained with the correlation of Assael et al.[90] as a function of density ρ. ●, this work, obtained by adjustment of two coefficients to minimize the difference between the densities obtained from the MEMS and values obtained from the correlation of Assael et al.[90] with our experimental temperatures and pressures; —, ref 126; gray diamond, ref 127; gray filled diamond, ref 136; gray asterisk, ref 128; □, ref 137; gray filled triangle, ref 138; gray circle, ref 129; ×, ref 139; asterisk, ref 140; ◇, ref 141; ■, ref 142; gray filled square, ref 143; gray +, ref 130; gray filled circle, ref 131; gray square, ref 132; △, ref 144; ▲, ref 133; and — —, expanded ($k = 2$) uncertainty of the correlation ref 90.

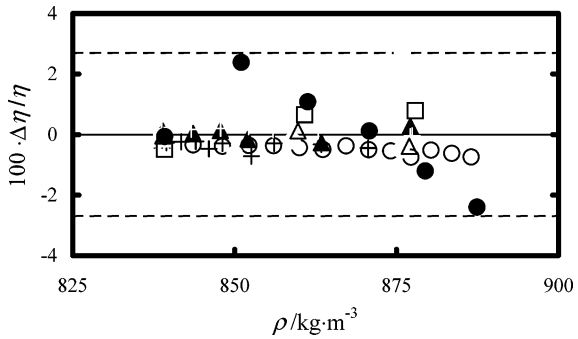

Figure 10. Fractional deviations $\Delta\eta = \eta(\text{expt}) - \eta(\text{calcd})$ of the experimental viscosities η(expt) of methylbenzene at $T = 323.15$ K from values η(calcd) obtained with the correlation of Assael et al.[90] as a function of density ρ. ●, this work, obtained by adjustment of one coefficient to minimize the difference between the viscosities obtained from the MEMS and values obtained from the correlation of Assael et al.[90] with our experimental temperatures and pressures; +, ref 127; ▲, ref 133; gray filled circle, ref 131; gray filled square, ref 134; gray circle, ref 129; asterisk, ref 146; gray +, ref 130; gray square, ref 132; △, ref 144; □, ref 148; and — —, expanded ($k = 2$) uncertainty of the correlation ref 90.

densities estimated from the eq 26 for the MEMS are listed in Table 2 and shown in Figure 10 as relative deviations from the correlation of Assael et al.[90] along with measurements reported in refs 127, 129−134, 144, and 148. The correlation of Assael et al.[90] has an estimated expanded ($k = 2$) uncertainty in viscosity of about 2.7 % and is shown in Figure 10 with a broken line. In Figure 10, our results (shown with solid circles) lie within ± 3 % of ref 90 and the literature values. Again, we take the average of the absolute differences of ± 1.2 % as a measure of the anticipated precision in the measurements of viscosity.

Finally, we note that in eqs 13 and 28 we have assumed the C_i, with $i = 1$, 2, and 3 are independent of T, p, η, and ρ. The consequences of these assumptions for the petroleum reservoir application will be discussed further below.

Results and Discussion

The resonance frequency $f_{r,f}$ and resonance line half-width g_f of the first eigenmode of the edge-supported plate that were measured while it was immersed in methylbenzene at a temperature of 373 K, and octane at temperatures between (323 and 423) K all at pressures below 68 MPa are listed in Table 2. The density and viscosity (also listed in Table 2) were obtained from eq 26 and eq 28, respectively, with the f_r and g of Table 2 combined with the C_1, C_2, and C_3 of Table 3 determined at a temperature of 323 K. In the analysis, the temperature and pressure dependence of the plate dimensions and the density and elastic constants of silicon were included as described previously. The density obtained from eq 26 with the MEMS $f_{r,f}$ was used in eq 28 to determine viscosity. Small corrections have been applied to the reported viscosity and density to reduce all values to the stated temperature for each isotherm. The combined expanded uncertainties (listed in Table 2) are for a coverage factor $k = 2$, assuming that a normal distribution is a confidence interval of about 0.95, and were obtained by combining in-quadrature standard uncertainties arising from the transducer calibration with $(\partial\eta/\partial T)_p$ and $(\partial\eta/\partial p)_T$ for viscosity and $(\partial\rho/\partial T)_p$ with $(\partial\rho/\partial p)_T$ for density. For the viscosity we have also included the uncertainty in density obtained from eq 13. Not surprisingly, for both density and viscosity the major source of uncertainty arises from the uncertainty in the calibration. Based on the absolute average errors obtained from the calibration, the uncertainty for density and viscosity are 0.1 % and 1.2 %, respectively. The next most significant and quantifiable contributions to the uncertainties arises from the quantities $(\partial\eta/\partial p)_T$ for viscosity and $(\partial\rho/\partial p)_T$ for density. These derivatives were estimated from a combination of our results and the uncertainties in the pressure measurement δp listed in Table 2. The contribution to the uncertainty in viscosity $\delta\eta$ from δp was less than 0.15 mPa·s (about 0.02 %), and $\delta\eta$ decreased with increasing temperature while the density error $\delta\rho$ from δp was less than 0.05 kg·m^{-3} (< 0.01 %). The contribution to the uncertainty from either $(\partial\eta/\partial T)_p$ or $(\partial\rho/\partial T)_p$ was estimated from a combination of our results and the uncertainties in the temperature measurement, δT, listed in Table 2. The contribution to $\delta\eta$ from δT was less than −0.02 mPa s (about $3\cdot10^{-4}$ %) and $\delta\rho \approx -3\cdot10^{-3}$ kg·m^{-3} (about $4\cdot10^{-4}$ %). Clearly, for our measurements the uncertainty with which the pressure is measured is more significant than the uncertainty of temperature. In the absence of a chemical analysis for these fluids, the contribution to the uncertainty arising from the uncertainty in composition was assumed to be negligible. The working equations explicitly assume that density and viscosity are represented by independent equations. In the absence of sufficient additional measurements with fluids of different densities and viscosities to determine the uncertainty from this source, we have also assumed that our zeroth order model contributes nothing to the estimated error.

The densities of methylbenzene obtained at a temperature of 373 K are listed in Table 2 and shown in Figure 11 as relative deviations from the values predicted from the correlation of Assael et al.[90] All deviations are between (0.2 and 0.4) % above ref 90 but agree with the correlation within a multiple of 1.1 times the combined uncertainty. Densities obtained from refs 135−144 are also shown in Figure 11, and except for the measurements of Gouel[135] that differ systematically by about −0.4 %, they lie within (−0.1 and 0.15) % of ref 90, which is within the estimated expanded uncertainty. These results show that for a fluid, with viscosity of order 1 mPa·s at temperatures in the range (323 to 373) K, the C_1 and C_2 can be considered independent of temperature. The viscosities obtained for methylbenzene are listed in Table 2 and shown in Figure 12 as deviations from the values obtained from the correlation of Assael et al.[90] along with the values from refs 143−148 at this

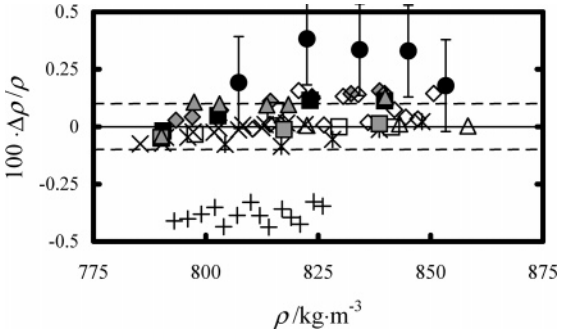

Figure 11. Fractional deviations $\Delta\rho = \rho(\text{expt}) - \rho(\text{calcd})$ of the experimental densities ρ(expt) of methylbenzene at $T \approx 373.15$ K from values ρ(calcd) obtained with the correlation of Assael et al.[90] as a function of density ρ. ●, this work, with error bars representing the expanded uncertainty, determined by adjustment of two coefficients to minimize the difference between the densities obtained from the MEMS and values obtained from the correlation of Assael et al.[90] with our experimental temperatures and pressures; +, ref 135; gray filled diamond, ref 136; □, ref 137; gray filled triangle, ref 138; ×, ref 139; asterisk, ref 140; ◇, ref 141; ■, ref 142; gray filled square, ref 143; △, ref 144; and − −, expanded ($k = 2$) uncertainty of the correlation ref 90.

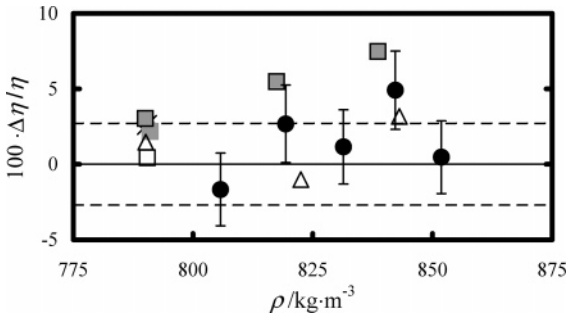

Figure 12. Fractional deviations $\Delta\eta = \eta(\text{expt}) - \eta(\text{calcd})$ of the experimentally determined viscosity η(expt) of methylbenzene at $T = 373.15$ K from values η(calcd) obtained with the correlation of Assael et al.[90] as a function of density ρ. ●, this work, with error bars representing the expanded uncertainty, determined by adjustment of one coefficient to minimize the difference between the viscosity obtained from the MEMS at $T = 323.15$ K and values obtained from the correlation of Assael et al.;[90] △, ref 144; gray filled square, ref 143; gray square, ref 145; asterisk, ref 146; ◆, ref 147; □, ref 148; and − −, expanded ($k = 2$) uncertainty of the correlation ref 90.

temperature; of these literature sources, only refs 143 and 144 extend to cover the pressure range of our measurements. Assael et al.[90] included in their correlation the measurements reported in refs 143 and 144, and our results lie within the estimated uncertainty of the measurements reported by Vieirra dos Santos and Nieto de Castro[144] and Dymond and Robertson.[145] These results demonstrate that for a fluid, with densities in the range (805 to 877) kg·m^{-3} at temperatures in the range (323 to 373) K, the constant C_3 can be considered independent of temperature.

The density of octane was determined at four temperatures of (323, 348, 373, and 423) K (using the C_1 and C_2 of Table 3 determined from measurements with methylbenzene at $T = 323$ K) and the results are listed in Table 2. Figures 13 through 16 show our results at temperatures from (323 to 423) K, respectively, with values from the literature as relative differences from the densities obtained with our measurement of temperature and pressure from the correlation of literature results reported by Span and Wagner[117] as a function of density ρ; ref 117 is identical to that reported by Span.[118] The correlation of Wagner and Span[117] has an uncertainty of ± 0.2 % at $p \leq 30$ MPa and ± 0.5 % at $p > 30$ MPa, which is depicted in Figures 13 through 16 with broken lines. The relative deviations would

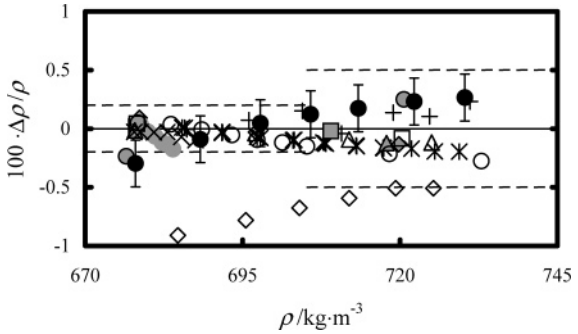

Figure 13. Fractional deviations $\Delta\rho = \rho(\text{expt}) - \rho(\text{calcd})$ of the experimental densities ρ(expt) of octane at $T = 323.15$ K from values ρ(calcd) estimated from the correlation of Span and Wagner[117] as a function of density ρ. ●, this work, with error bars representing the expanded uncertainty, determined with the calibration coefficients obtained at $T = 323.15$ K when immersed in methylbenzene; △, ref 149; gray filled diamond, ref 150; □, ref 151; asterisk, ref 152; gray circle, ref 153; +, ref 154; gray filled square, ref 155; gray filled triangle, ref 156; ◇, ref 157; ○, ref 133; gray filled circle, ref 158; ×, ref 159; and − −, uncertainty of the correlation ref 117.

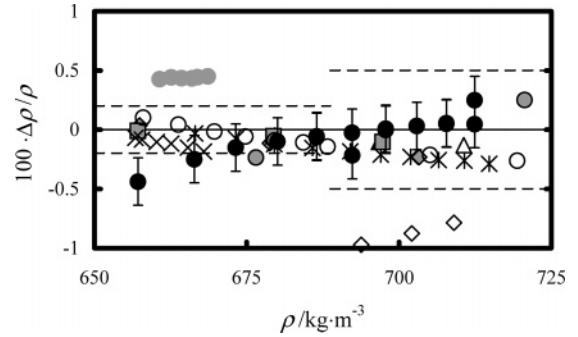

Figure 14. Fractional deviations $\Delta\rho = \rho(\text{expt}) - \rho(\text{calcd})$ of the experimental densities ρ(expt) of octane at $T = 348.15$ K from values ρ(calcd) estimated from the correlation of Span and Wagner[117] as a function of density ρ. ●, this work, with error bars representing the expanded uncertainty, determined with the calibration coefficients obtained at $T = 323.15$ K when immersed in methylbenzene; △, ref 149; gray filled diamond, ref 150; asterisk, ref 152; gray circle, ref 153; gray filled square, ref 155; ◇, ref 157; ○, ref 133; gray filled circle, ref 158; ×, ref 159; and − −, uncertainty of the correlation ref 117.

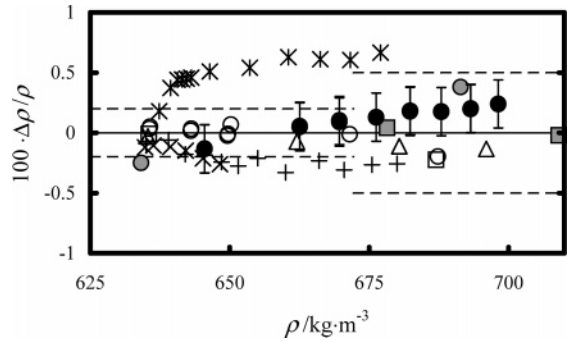

Figure 15. Fractional deviations $\Delta\rho = \rho(\text{expt}) - \rho(\text{calcd})$ of the experimental densities ρ(expt) of octane at $T = 373.15$ K from values ρ(calcd) estimated from the correlation of Span and Wagner[117] as a function of density ρ. ●, this work, with error bars representing the expanded uncertainty, determined with the calibration coefficients obtained at $T = 323.15$ K when immersed in methylbenzene; △, ref 149; □, ref 151; asterisk, ref 160; +, ref 135; gray filled square, ref 151; gray filled circle, ref 158; ◇, ref 157; ○, ref 161; ×, ref 159; and − −, uncertainty of the correlation ref 117.

not have differed significantly had the correlation of Cibulka and Hnedkovský[119] combined with a reference density given by Cibulka[120] at the vapor pressure reported by Ambrose and

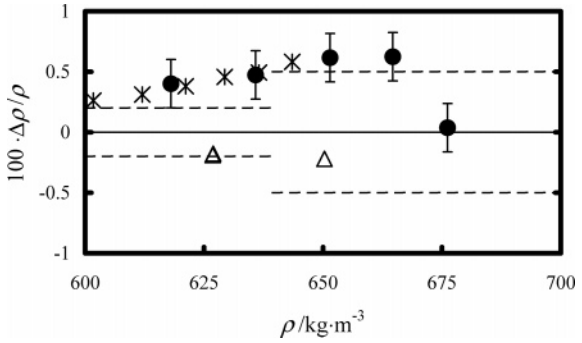

Figure 16. Fractional deviations $\Delta\rho = \rho(\text{expt}) - \rho(\text{calcd})$ of the experimental densities ρ(expt) of octane at $T = 423.15$ K from values ρ(calcd) estimated from the correlation of Span and Wagner[117] as a function of density ρ. ●, this work, with error bars representing the expanded uncertainty, determined with the calibration coefficients obtained at $T =$ 323.15 K when immersed in methylbenzene; △, ref 149; asterisk, ref 160; ◇, ref 157; and − −, uncertainty of the correlation ref 117.

Walton[121] been used. At $T = 323$ K (shown in Figure 13), our results lie between (−0.3 and 0.3) % of ref 117 and within our estimated expanded uncertainty as do all the literature measurements expect for that reported by Kiran and Sen.[157] Our results show the same density dependence as the results reported by Kiran and Sen,[157] albeit with an offset, while all other literature values differ from ref 117 by less than ± 0.3 %. At a temperature of 348 K (shown in Figure 14), our results lie between (−0.4 and 0.3) % of the values obtained from both ref 117 and the literature values except the measurements reported by Kiran and Sen[157] that lie about 1 % below ref 117. The results obtained at a temperature of 373 K (shown in Figure 15) lie between (−0.1 and 0.2) % of ref 117 while the literature values lie within (−0.3 and 0.5) % of ref 117. At $T = 423$ K, where the literature values differ from ref 117 by between (−0.2 and 0.5) %, our results agree (as shown in Figure 16) with those obtained from ref 117 within the assigned expanded uncertainty. The densities reported by Caudwell,[149] which were obtained using a vibrating wire with a mass suspended from one end, are shown in Figure 13 through 16. These differ from our results by about 1.5 times the estimated expanded uncertainty in our measurements except at a temperature of 423 K where the two sets of results differ by about 0.6 %. The relative deviations (shown in Figures 13 through 16) have no significant temperature dependence and, therefore, cannot be attributed to thermal annealing of the packaged transducer that has subsequently altered the mechanical response of the transducer and thus the C_i.

The viscosity of octane determined over the temperature range (323, 348, 373, and 423) K from eq 28 with C_3 of Table 3 using the density given in Table 2 is also listed in Table 2. Figures 17 through 20 show our results with values from the literature as relative differences from viscosities obtained with the correlation of Huber et al.[122] that used the correlation for density reported by Span and Wagner.[117] Had we used the viscosity correlation reported by Assael et al.,[123] the baseline in Figures 17 through 20 would have changed by no more than 2 %, which is equivalent to the uncertainty in the viscosity obtained from the correlation of Huber et al.[122] At temperatures between (323 and 373) K at all pressures, our results lie within the combined uncertainty of the correlation and our results. At $T = 323$ K (shown in Figure 17), our results deviate (albeit with a systematic undulation) from ref 122 by between (−2.5 and 3.5) % while the literature results lie within (−3 and 1) % of ref 122 except for those reported by Kiran and Sen,[157] which lie between (3 and 6) % above ref 122. At $T = 348$ K (shown

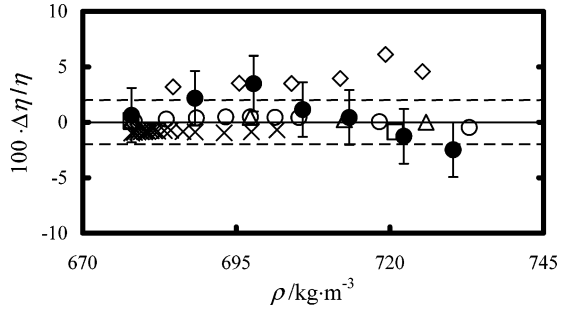

Figure 17. Fractional deviations $\Delta\eta = \eta(\text{expt}) - \eta(\text{calcd})$ of the experimental viscosities η(expt) of octane at $T = 323.15$ K from values η(calcd) obtained with the correlation of Huber et al.[122] as a function of density ρ. The density required in ref 122 was taken from ref 117. ●, this work, with error bars representing the expanded uncertainty, determined with the calibration coefficients obtained at $T =$ 323.15 K when immersed in methylbenzene and the densities of Table 2; ○, ref 133; ◇, ref 157; △, ref 149; □, ref 151; ×, ref 162; and − −, uncertainty of the correlation ref 122.

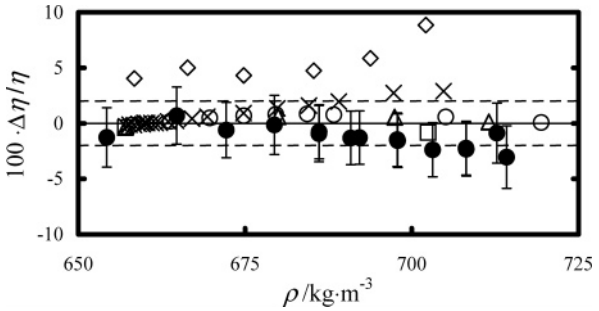

Figure 18. Fractional deviations $\Delta\eta = \eta(\text{expt}) - \eta(\text{calcd})$ of the experimental viscosities η(expt) of octane at $T = 348.15$ K from values η(calcd) obtained with the correlation of Huber et al.[122] as a function of density ρ. The density required in ref 122 was taken from ref 117. ●, this work, with error bars representing the expanded uncertainty, determined with the calibration coefficients obtained at $T = 323.15$ K, when immersed in methylbenzene and the densities from Table 2; ○, ref 133; ◇, ref 157; △, ref 149; □, ref 151; ×, ref 162; and − − − −, uncertainty of the correlation ref 122.

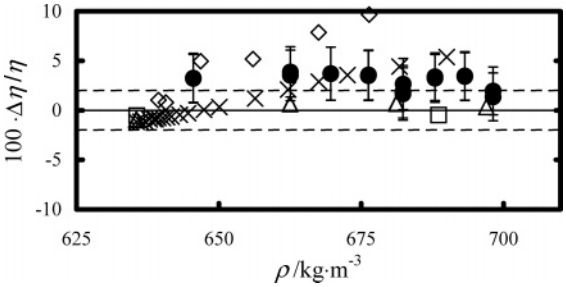

Figure 19. Fractional deviations $\Delta\eta = \eta(\text{expt}) - \eta(\text{calcd})$ of the experimental viscosities η(expt) of octane at $T = 373.15$ K from values η(calcd) obtained with the correlation of Huber et al.[122] as a function of density ρ. The density required in ref 122 was obtained from ref 117. ●, this work, with error bars representing the expanded uncertainty, determined with the calibration coefficients obtained at $T = 323.15$ K, when immersed in methylbenzene, and the densities from Table 2.; ◇, ref 157; △, ref 149; □, ref 151; ×, ref 162; and − −, uncertainty of the correlation ref 122.

in Figure 18), our results deviate between (−3 and 1) % from ref 122 and lie within 2 % of all literature values except those reported by Kiran and Sen,[157] which deviate from ref 122 by 5 % at the lowest pressure to about 10 % at the highest pressure studied. The results obtained at $T = 373$ K (shown in Figure 19) lie between (1 and 4) % above ref 122, agree with the most recent measurements obtained with a vibrating wire,[149] and lie within 1.5 times the assigned uncertainty of all other literatures values except those reported by Kiran and Sen,[157] which deviate

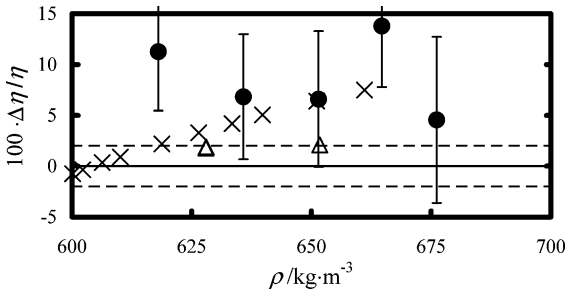

Figure 20. Fractional deviations $\Delta\eta = \eta(\text{expt}) - \eta(\text{calcd})$ of the experimental viscosities η(expt) of octane at $T = 423.15$ K from values η(calcd) obtained with the correlation of Huber et al.[122] as a function of density ρ. The density required in ref 122 was obtained from ref 117. ●, this work, with error bars representing the expanded uncertainty, determined with the calibration coefficients obtained at $T = 323.15$ K, when immersed in methylbenzene, and the densities of Table 2; △, ref 149; ×, ref 162; and − −, uncertainty of the correlation ref 122.

up to 10 % from ref 122. Finally, at $T = 423$ K, our results have an expanded uncertainty of about 6 %. This arises from the larger {by a factor of between (5 and 10)} error in the resonance frequency and the resonance half-line width that we attributed to a lower signal-to-noise ratio at this temperature. At this temperature, our values of viscosity are shown as relative fractional deviations from ref 122 in Figure 20, and they lie between (6 and 14) % above ref 122. The viscosity reported by Caudwell[149] and obtained with a vibrating wire viscometer agrees within the estimated expanded uncertainty of our results, as do the measurements of Agaev and Golubev.[162] The latter differ from ref 122 by about −1 % at the lowest density, a difference that increases with increasing density to 7 % at the highest density.

The measurements were performed first with octane at temperatures of (348, 373, and 323) K followed by methylbenzene at temperatures of (323 and 373) K, and finally octane at a temperature of 423 K. It is entirely plausible the procedure used to clean the apparatus between measurements with different fluids was inadequate and, because this reduced the chemical purity from that cited by the supplier, introduced an additional uncertainty in the measurements. The effect of this source of uncertainty on the measured density and viscosity can be estimated. Contamination could have occurred for the measurements with methylbenzene that were performed after those on octane or when the fluid was changed from methylbenzene to octane. In either of these cases, $(1/\eta)(\partial\eta/\partial x)_{T,p} \approx 0.4$ and implies that a mole fraction $x = 0.3$ of the contaminant would be required to introduce an uncertainty in viscosity of ± 10 % while $(1/\rho)(\partial\rho/\partial x)_{T,p} \approx 0.3$ and suggests that $x = 0.03$ would be required to introduce an error ± 1 % in density. These, albeit large, mole fractions of impurity cannot be ruled out in the absence of chemical composition measurements but appear implausible because of the consistency of the results presented here with literature correlations of data that are independent of ours.

If we assume the correlations of the measurements reported in the literature for each fluid and thermophysical property are for all intents and purposes exact, the relative deviations shown in Figures 11 to 20 might arise from one or more of the following plausible sources of error in our experiment: first, the simplicity of eq 26 that was obtained with the assumption that density can be represented by an expression independent of viscosity (the inviscid assumption used to obtain eq 13); second, the simplicity of eq 28; and third, the arbitrary use of only three calibration parameters two for density (eq 26) and one for viscosity (eq 28).

For the fluids investigated and reported in this paper, the density varied between (619 and 890) kg·m^{-3} and viscosity over the range (0.205 to 0.711) mPa·s. To investigate the effect of varying viscosity on the measured density, preliminary measurements were performed with research grade argon obtained from Praxair with a mole fraction purity greater than 0.999999. The resonance frequency and half line-width were measured at a temperature of 323.151 K at pressures between (13.8 and 68.4) MPa, and eqs 26 and 28 were used with the coefficients of Table 3, determined with methylbenzene, to obtain both density and viscosity. The densities so determined were about 4 % below the correlation of Tegeler et al.,[124] while the viscosity was 5 % above the correlation of Lemmon and Jacobsen.[125] This demonstrates the naivety of eqs 13 and 28. In a future paper, we will report measurements with fluids of viscosities between (0.01 and 300) mPa·s and densities in the range (1 to 1850) kg·m^{-3}. These results will be used to examine further the applicability of the working equations described in this paper, particularly with respect to order of magnitude variations in viscosity, and also present, as we alluded to above, a complete solution coupling both density and viscosity. Presumably, the deviations of our measured densities and viscosities from the accepted literatures values will decrease when these properties are obtained from the complex frequency with other working equations.[103,109,111]

Conclusion

Our intent was to fabricate a densimeter/viscometer for the simultaneous measurement of density and viscosity that can operate at temperatures below 473 K and pressures up to 200 MPa and provide densities with an uncertainty of ± 1 % and viscosities with an uncertainty of ± 10 %. The temperature and pressure range represent those experienced in petroleum reservoirs and the production system while the accuracy in both properties are sufficient to guide value and exploitation calculations with sufficient rigor. The geometry of the device was also constrained by the requirements to derive working equations for a well-defined shape of known dimensions and, when fabricated by the methods of MEMS, necessarily precluded the use of curved surfaces. The operating environment, geometric constraints, fabrication process, and desired uncertainty in density and viscosity meant that the robustness of the device was given a higher priority in the design than assigned to accuracy. Nevertheless, the complex frequency determined when the MEMS was immersed in methylbenzene at a temperature of 373 K and octane at temperatures between (323 and 423) K and pressure below 68 MPa provided density and viscosity with an estimated relative combined expanded ($k = 2$) uncertainty, including the calibration, of about ± 0.2 % for density and < ± 2.5 % for viscosity and about ± 6 % at $T = 423$ K. At $T < 423$ K, the measured density differed by ± 0.3 %, and the viscosity differed by less than ± 5 % from literature values. The literature values were obtained from either accepted correlations or measurements obtained from experimental techniques that utilize different principles and thus have quite different sources of systematic error. At a temperature of 423 K, the measured viscosity differed by less than 13 % from literature values while the density differed by less than 0.5 %. It is plausible at a temperature of 423 K the packaged MEMS had mechanical characteristics that are significantly different than they are at lower temperatures. Presumably the differences between density and viscosity obtained with the MEMS and those from other experimental methods will decrease as the working equations for the MEMS are improved.[103,109,111]

Within the constraints of the upper operating pressure determined by the positive displacement pump and the upper operating temperature determined by adhesive used in the packaging, the goal of determining density to ± 1 % and viscosity to ± 10 % in viscosity has been achieved.

Acknowledgment

The authors acknowledge Christopher Harrison (Schlumberger-Doll Research) for his preliminary measurements of the amplitude of plate motion and effect of separation from a boundary, Gerry Meeten (Schlumberger Cambridge Research) for his assistance with the project, and Kai Hsu (Schlumberger Technology Corporation) for his assistance in the preparation of Figure 6.

Literature Cited

(1) Johnson, J. F.; Martin, J. R.; Porter, R. S. *Physical Methods of Chemistry, Part VI*; Weissberger, A. L., Rossiter, B. W., Eds.; Interscience: New York, 1977; p 63.

(2) Künzel, W.; van Wijk, H. F.; Marsh, K. N. Viscosity. In *Recommended Reference Materials for the Realization of Physicochemical Properties*; Marsh, K. N., Ed.; Blackwell Scientific for International Union of Pure and Applied Chemistry: Oxford, U.K., 1987; pp 45−72.

(3) Nieuwoudt, J. C.; Shankland, I. R. Oscillating-body viscometers. In *Experimental Thermodynamics Vol. III, Measurement of the Transport Properties of Fluids*; Wakeham, W. A., Nagashima, A., Sengers, J. V., Eds.; Blackwell Scientific for International Union of Pure and Applied Chemistry: Oxford, U.K., 1991; Chapter 2, pp 9−48.

(4) Kawata, M.; Kurase, K.; Nagashima, A.; Yoshida, K. Capillary viscometers. In *Experimental Thermodynamics Vol. III, Measurement of the Transport Properties of Fluids*; Wakeham, W. A., Nagashima, A., Sengers, J. V., Eds.; Blackwell Scientific for International Union of Pure and Applied Chemistry: Oxford, U.K., 1991; Chapter 3, pp 51−75.

(5) Kawata, M.; Kurase, K.; Nagashima, A.; Yoshida, K.; Isdale, J. D. Falling-body viscometers. In *Experimental Thermodynamics Vol. III, Measurement of the Transport Properties of Fluids*; Wakeham, W. A., Nagashima, A., Sengers, J. V., Eds.; Blackwell Scientific for International Union of Pure and Applied Chemistry: Oxford, U.K., 1991; Chapter 5, pp 97−110.

(6) Diller, D. E.; van der Gulik, P. S. Vibrating viscometers In *Experimental Thermodynamics Vol. III, Measurement of the Transport Properties of Fluids*; Wakeham, W. A., Nagashima, A., Sengers, J. V., Eds.; Blackwell Scientific for International Union of Pure and Applied Chemistry: Oxford, U.K., 1991; Chapter 4, pp 79−94.

(7) Wagner, W.; Kleinrahm, R.; Lösch, H. W.; Watson, J. T. R.; Majer, V.; Pádua, A. A. H.; Woolf, L. A.; Hoslte, J. C.; de Figueiredo Palavara, A. M.; Fujii, K.; Stansfeld, J. W. Density. In *Experimental Thermodynamics Vol. VI, Measurement of the Thermodynamic Properties of Single Phases*; Goodwin, A. R. H., Marsh, K. N., Wakeham W. A., Eds.; Elsevier for International Union of Pure and Applied Chemistry: Amsterdam, 2003; Chapter 5, pp 127−235.

(8) Wagner, W.; Kleinrahm, R. Densimeters for very accurate density measurements of fluids over large ranges of temperature, pressure, and density. *Metrologia* **2004**, *41*, S24−S39.

(9) Kuramoto, N.; Fujii, K.; Waseda A. Accurate density measurements of reference liquids by a magnetic suspension balance. *Metrologia* **2004**, *41*, S84−S94.

(10) Fujii, K. Absolute density standards. In *Experimental Thermodynamics Vol. VI, Measurement of the Thermodynamic Properties of Single Phases*; Goodwin, A. R. H., Marsh, K. N., Wakeham, W. A., Eds.; Elsevier for International Union of Pure and Applied Chemistry: Amsterdam, 2003; Chapter 5, pp 191−208.

(11) Fujii, K. Present state of the solid and liquid density standards. *Metrologia* **2004**, *41*, S1−S15.

(12) Majer, V.; Pádua, A. A. H. Measurement of density with vibrating bodies. In *Experimental Thermodynamics Vol. VI, Measurement of the Thermodynamic Properties of Single Phases*; Goodwin, A. R. H., Marsh, K. N., Wakeham, W. A., Eds.; Elsevier for International Union of Pure and Applied Chemistry: Amsterdam, 2003; Chapter 5, pp 158−168.

(13) Stansfeld, J. W. In situ density measurement. In *Experimental Thermodynamics Vol. VI, Measurement of the Thermodynamic Properties of Single Phases*; Goodwin, A. R. H., Marsh, K. N., Wakeham, W. A., Eds.; Elsevier for International Union of Pure and Applied Chemistry: Amsterdam, 2003; Chapter 5, pp 208−225.

(14) Romoscanu, A. I.; Sayir, M. B.; Häusler, K.; Servais, C. High-frequency probe for the measurement of the complex viscosity of liquids. *Meas. Sci. Technol*. **2003**, *14*, 451−462.

(15) Martin, B. A.; Wenzel, S. W.; White R. M. Viscosity and density sensing with ultrasonic plate waves. *Sens. Actuators A* **1990**, *21−23*, 704−708

(16) Li, K. K.; Schneider, A.; Abraham, R. L. Instrument for the remote determination of viscosity and density in hostile environments. *Rev. Sci. Instrum.* **1992**, *63*, 4192−4195.

(17) Woodward, J. G. A vibrating plates viscometer. *J. Acoust. Soc. Am*. **1953**, *25*, 147−151.

(18) Andrews, M. K.; Harris, P. D. Damping and a gas viscosity measurements using a micostructure. *Sens. Actuators A* **1995**, *49*, 103−108.

(19) Martin, S. J.; Butler, M. A.; Spates, J. J.; Mitchell, M. A.; Schubert, W. K. Flexural plate wave resonator excited with Lorentz forces. *J. Appl. Phys.* **1998**, *83*, 4589−4601.

(20) Enoksson, P.; Stemme, G.; Stemme, E. Fluid density sensor based on resonance vibration. *Sens. Actuators A* **1995**, *46−47*, 327−331.

(21) Corman, T.; Enoksson, P.; Norén, K.; Stemme, G. A low-pressure encapsulated resonant fluid density sensor with feedback control electronics. *Meas. Sci. Technol*. **2000**, *11*, 205−211.

(22) Zhang, Y.; Tadigadapa, S. Najafi, N. A micromachined coriolis-force-based mass flowmeter for direct mass flow and fluid density measurement. *Transducers '01 Eurosensors XV*; Proceedings of the 11th International Conference on Solid-State Sensors and Actuators, Munich, Germany, June 10−14, 2001.

(23) Binning, G.; Quate, C. F.; Gerber, C. Atomic Force Microscope. *Phys. Rev. Lett.* **1986**, *56*, 930−933.

(24) Weigert, S.; Dreier, M.; Hegner, M. Frequency shifts of cantilevers vibrating in various media. *Appl. Phys. Lett*. **1996**, *69*, 2834−2836.

(25) Oden, P. I.; Chen, G. Y.; Steele, R. A.; Warmack, R. J.; Thundat. T. Viscous drag measurements utilizing microfabricated cantilevers. *Appl. Phys. Lett*. **1996**, *68* (26), 3814−3816.

(26) Kirstein, S.; Mertesdorf, M.; Schönhoff, M. The influence of a viscous fluid on the vibration dynamics of scanning near-field optical microscopy fiber probes and atomic force microscopy cantilevers. *J. Appl. Phys.* **1998**, *84*, 1782−1790.

(27) Patois, R.; Vairac, P.; Cretin, B. Measurement of fluid properties with a near-field acoustic sensor. *Appl. Phys. Lett*. **1999**, *75*, 295−297.

(28) Bergaud, C.; Nicu, L. Viscosity measurements based on experimental investigations of composite cantilever beam eigenfrequencies in viscous media. *Rev. Sci. Instrum.* **2000**, *71*, 2487−2491.

(29) Patois, R.; Vairac, P.; Cretin, B. Near-field acoustic densimeter and viscosimeter. *Rev Sci. Instrum*. **2000**, *71*, 3860−3863.

(30) Boskovic, S.; Chon, J. W. M.; Mulvaney, P.; Sader, J. E. Rheological measurements using microcantilevers. *J. Rheol*. **2002**, *46*, 891−899.

(31) Ahmed, N.; Nino, D. F.; Moy, V. T. Measurement of solution viscosity by atomic force microscopy. *Rev Sci. Instrum*. **2001**, *72*, 2731−2734.

(32) Vidic, A.; Then, D.; Ziegler, Ch. A new cantilever system for gas and liquid sensing. *Ultramicroscopy* **2003**, *97*, 407−416.

(33) Maali, A.; Hurth, C.; Boisgard, R.; Jai, C.; Cohen-Bouhacina, T.; Aimé, J.-P. Hydrodynamics of oscillating atomic force microscopy cantilevers in viscous fluids. *J. Appl. Phys.* **2005**, *97*, 074907-1, 074907-6.

(34) Walters, D. A.; Cleveland, J. P.; Thomson, N. H.; Hansma, P. K., Wendman, M. A.; Gurley, G.; Elings, V. Short cantilevers for atomic force microscopy. *Rev. Sci. Instrum*. **1996**, *67*, 3583−3590.

(35) Passiana, A.; Warmacka, R. J.; Wiga, A.; Farahia, R. H.; Meriaudeaub, F.; Ferrella, T. L.; Thundata, T. Observation of Knudsen effect with microcantilevers. *Ultramicroscopy* **2003**, *97*, 401−406.

(36) Su, Y.; Evans, A. G. R.; Brunnschweiler, A. Micromachined silicon cantilever paddles with piezoresistive readout for flow sensing. *J. Micromech. Microeng*. **1996**, *6*, 69−72.

(37) Baek, C.-W.; Kim, Y.-K.; Ahn, Y.; Kim, Y.-H. Measurement of the mechanical properties of electroplated gold thin films using micromachined beam structures. *Sens. Actuators A* **2005**, *117*, 17−27.

(38) Klesewetter, L.; Zhang, J -M.; Houdeau, D.; Steckenbom, A. Determination of Young's moduli of micromechanical thin films using the resonance method. *Sens. Actuators A* **1992**, *35*, 153−159.

(39) França, D. R.; Blouin, A. Measurement of Young's modulus and Poisson's ratio in silicon wafer. *Meas. Sci. Technol*. **2004**, *15*, 859−868.

(40) Thundat, T.; Wachter, E. A.; Sharp, S. L.; Warmack, R. J. Detection of mercury vapor using resonating microcantilevers. *Appl. Phys. Let*. **1995**, *66*, 1695−1697

(41) Baller, M. K.; Lang, H. P.; Fritz, J.; Gerber, Ch.;. Gimzewski, J. K.; Drechsler, U.; Rothuizen, H.; Despont, M.; Vettiger, P.; Battiston, F. M.; Ramseyer, J. P.; Fornaro, P.; Meyer, E.; Güntherodt, H.-J. A cantilever array-based artificial nose. *Ultramicroscopy* **2000**, *82*, 1−9.

(42) Battison, F. M.; Ramseyer, J.-P.; Lang, H. P.; Baller, M. K.; Gerber, Ch.; Gimzewski, J. K.; Meyer, E.; Güntherodt, H.-J. A chemical based on a microfabricated cantilever array with simultaneous resonance-frequency and bending readout. *Sens. Actuators B* **2001**, *77*, 122−131.

(43) Xu, X.; Thundat, T, G.; Briwn, G. M.; Ji, H.-F. Detection of Hg^{2+} Using microcantilever sensors. *Anal. Chem*. **2002**, *74*, 3611 3615.

(44) Rogers, B.; Manning, L.; Jones, M.; Sulchek, T.; Murray, K.; Beneschott, B.; Adams, J. D.; Cavazos, H.; Minne, S. C. Mercury vapor detection with a self-sensing, resonating piezoelectric cantilever. *Rev. Sci. Instrum.* **2003**, *74*, 4899−4901.

(45) Moulin, A. M.; O'Shea, S. J.; Welland, M. E. Microcantilever-based biosensors. *Ultramicroscopy* **2000**, *82*, 23−31.

(46) Raiteri, R.; Grattarola, M.; Butt, H.-J.; Skládal, P. Micromechanical cantilever-based biosensors. *Sens. Actuators B* **2001**, *79*, 115−126.

(47) Jalili, N.; Laxminarayana, K. A review of atomic force microscopy imaging systems: application to molecular metrology and biological sciences. *Mechatronics* **2004**, *14*, 907−945.

(48) Hagleitner, C.; Hierlemann, A.; Lange, D.; Kummer, A.; Kerness, N.; Brand, O.; Baltes, H. Smart single-chip gas sensor microsystem. *Nature* **2001**, *414*, 293−296.

(49) Godin, M.; Tabard-Cossa, V.; Grütter, P.; Williams, P. Quantitative surface stress measurements using a microcantilever, *Appl. Phys. Lett*. **2001**, *79*, 551−553.

(50) Sader, J. E. Surface stress induced deflections of cantilever plates with applications to the atomic force microscope: rectangular plates *J. Appl. Phys.* **2001**, *89*, 2911−2921.

(51) Shieh, J.; Huber, J. E.; Fleck, N. A.; Ashby, M. F. The selection of sensors. *Prog. Mater. Sci*. **2001**, *46*, 461−504.

(52) Judy, J. W. Microelectromechanical systems (MEMS): fabrication, design and applications. *Smart Mater. Struct*. **2001**, *10*, 1115−1134.

(53) Werner, M. R.; Fahrner, W. R. Review on materials, microsensors, systems, and devices for high-temperature and harsh-environment applications. *IEEE Trans. 1nd. Electr*. **2001**, *48*, 249−257.

(54) Donzier, E., Lefort, O., Spirkovitvh, S., Baillieu, F. Integrated magnetic field sensor. *Sens. Actuators A* **1991**, *25*−*27*, 357−361.

(55) Lundstrum, R.; Goodwin, A. R. H.; Hsu, K.; Frels, M.; Caudwell, D.; Trusler, J. P. M.; Marsh, K. N. Measurement of the viscosity and density of two reference fluids, with nominal viscosities at $T = 298$ K and $p = 0.1$ MPa of (16 and 29) mPa•s, at temperatures between (298 and 398) K and pressures below 55 MPa. *J. Chem. Eng. Data* **2005**, *50*, 1377−1388.

(56) Sopkow, T.; Hsu, K.; Goodwin, A. R. H. Vibrating wire viscometer with nominal wire diameter of 0.15 mm: measurement of the viscosity of two certified reference fluids, with nominal viscosities at $T = 298$ K and $p = 0.1$ MPa of (16 and 29) mPa•s, at temperatures between (298 and 353) K and pressures below 55 MPa. *J. Chem. Eng. Data* **2005**, *50*, 1732−1735.

(57) Jakeways, C. V.; Goodwin, A. R. H. The viscosity and density of 1-propene,1,1,2,3,3,3-hexafluoro-oxidized-polymd and polydimethylsiloxane at temperatures from 313 K to 373 K and a pressure of 0.1 MPa. *J. Chem. Thermodyn*. **2005**, *37*, 1093−1097.

(58) Goodwin, A. R. H.; Fitt, A.; Ronaldson, K.; Wakeham, W. A. A vibrating plate fabricated with the methods of micro electro mechanical systems (MEMS): measurement of the density and viscosity of argon at temperatures between 323 K and 423 K at pressures up to 68 MPa. *Int J. Thermophys.* (submitted for publication).

(59) Ronaldson, K.; Fitt, A.; Goodwin, A. R. H.; Wakeham, W. Transversely oscillating MEMS viscometer. *Int. J. Thermophys*. (to be submitted).

(60) Lindholm, U. S.; Kana, D. D.; Chu, W.-H.; Abramson, H. N. Elastic vibrations characteristics of cantilever plates in water. *J. Ship Res*. **1965**, *9*, 11−36.

(61) Leissa, A. W. Vibration of Plates. NASA Special Publication 160; 1969.

(62) Elmer, F.-J.; Dreier, M. Eigenfrequencies of a rectangular atomic force microscope cantilever in a medium. *J. Appl. Phys*. **1997**, *81*, 7709−7714.

(63) Sadar, J. E. Frequency response of cantilever beams immersed in viscous fluids with applications to the atomic force microscope. *J. Appl. Phys.* **1998**, *84*, 64−76.

(64) Chang, T.-P.; Liu, M.-F. On the natural frequency of a rectangular isotropic plate in contact with fluid. *J. Sound Vib*. **2000**, *236*, 547−553

(65) Dareinga, D. W.; Thundat, T.; Jeon, S.; Nicholson, M. Modal analysis of microcantilever sensors with environmental damping. *J. Appl. Phys*. **2005**, *97*, 084902

(66) Chon, J. W. M.; Mulvaney, P.; Sadar, J. E. Experimental validation of theoretical models for the frequency response of atomic force microscope cantilever beams immersed in fluids. *J. Appl. Phys.* **2000**, *87*, 3978−3988.

(67) Baker, W. E.; Woolam, W. E.; Young, D. Air and internal damping of thin cantilever beams. *Int. J. Mech. Sci.* **1967**, *9*, 743−766.

(68) Gysin, U.; Rast, S.; Ruff, P.; Meyer, E.; Lee, D. W.; Vettiger, P.; Gerber, C. Temperature dependence of the force sensitivity of silicon cantilevers. *Phys. Rev. B* **2004**, *69*, 045403

(69) Sader, J. E.; Green, C. P. Torsional frequency response of cantilever beams immersed in viscous fluids with applications to the atomic force microscope. *J. Appl. Phys*. **2002**, *92*, 6262−6274.

(70) Landau, L. D.; Lifshitz, E. M. *Fluid Mechanics*; Pergamon: New York, 1959.

(71) Chen, G. Y.; Warmack, R. J.; Thundat, T.; Allison, D. P.; Huang, A. Resonance response of scanning force microscopy cantilevers. *Rev. Sci. Instrum*. **1984**, *65*, 2532−2537.

(72) Cumberbatch, E.; Wilks, G. An analysis of a vibrating element densitometer. *Math. Eng. Ind*. **1987**, *1* 47−66.

(73) Cumberbatch, E.; Fitt, A. *Mathematical Modelling: Case Studies from Industry*; Cambridge University Press: Cambridge, U.K., 2001; pp 66−79.

(74) Hinch, E. J. *Perturbation Methods*; Cambridge University Press: Cambridge, U.K., 1991; pp 87−90.

(75) Van Dyke, M. *Perturbation Methods in Fluid Mechanics*; Academic Press: London, U.K., 1964; pp 87−90.

(76) McSkimin, H. J. Measurement of elastic constants at low temperatures by means of ultrasonic waves—data for silicon and germanium single crystals, and fused silica. *J. Appl. Phys*. **1953**, *24*, 988−997.

(77) Nikanorov, S. P.; Burenkov, Yu. A.; Stepanov, A. V. *Sov. Phys. Solid State* **1971**, *13*, 2516−2519.

(78) Wortman, J. J.; Evans, R. A. Young's modulus, shear modulus and Poisson's ratio in silicon and germanium. *J. Appl. Phys.* **1965**, *36*, 153.

(79) Bettin, H.; Toth. H. Density comparisons of silicon samples by the pressure-of-flotation method at PTB. *Metrologia* **2004**, *41*, S52−S61

(80) Waseda, A.; Fujii, K. High precision density comparison measurement of silicon crystals by the pressure of flotation method. *Meas. Sci. Technol*. **2001**, *12*, 2039−2045.

(81) Waseda, A.; Fujii, K. Density comparison measurements of silicon crystals by a pressure-of-flotation method at NMIJ. *Metrologia* **2004**, *41*, S62−S67.

(82) Nye J. F.; Ed. *Physical Properties of Crystals*; Oxford University Press: Oxford, 1992.

(83) Swenson, C. A. Recommended values for the thermal expansivity of silicon from 0 to 1000 K, *J. Phys. Chem. Ref. Data* **1983**, *12*, 179−182.

(84) Okaji, M. Absolute thermal expansion measurements of single-crystal silicon in the range 300−1300 K with an interferometric dilatometer. *Int. J. Thermophys*. **1988**, *9*, 1101−1109.

(85) Desai, P. D. Thermodynamic properties of iron and silicon. *J. Phys. Chem. Ref. Data* **1986**, *15*, 967−983.

(86) Brugger, K. Thermodynamic definition of higher order elastic constants. *Phys. Rev.* **1964**, *133*, A1611−A1612.

(87) McSkimin, H. J.; Andreatch P., Jr. Elastic moduli of silicon vs hydrostatic pressure at 25.0 °C and 195.8 °C. *J. Appl. Phys*. **1964**, *35*, 2161−2165.

(88) McSkimin, H. J.; Andreatch P., Jr. Measurement of third-order moduli of silicon and germanium. *J. Appl. Phys.* **1964**, *35*, 3312−3319.

(89) Philip, J.; Breazeale, M. A. Temperature variation of some combinations of third-order elastic constants of silicon between 300 and 3 K. *J. Appl. Phys.* **1981**, *52*, 3383−3387.

(90) Assael, M. J.; Avelino, H. M. T.; Dalaouti, N. K.; Fareleira J. M. N. A.; Harris K. R. Reference correlation for the viscosity of liquid toluene from 213 to 373 K at pressures to 250 MPa. *Int. J. Thermophys*. **2001**, *22*, 789−799.

(91) Carlotti, G.; Doucet, L.; Dupeux, M. Elastic properties of silicon dioxide films deposited by chemical vapour deposition from tetraethylorthosilicate. *Thin Solid Films* **1997**, *296*, 102−105.

(92) Santucci, S.; Lozzi, L.; Passacantando, M.; Phani, A. R.; Palumbo, E.; Bracchitta, G.; De Tommasis, R.; Torsi. A.; Alfonsetti. R.; Moccia. G. Properties of stacked dielectric films composed of $SiO_2/Si_3N_4/SiO_2$. *J. Non-Cryst. Solids* **1999**, *245*, 224−231.

(93) Chinmulgund, M.; Inturi, R. B.; Barnard, J. A. Effect of Ar gas pressure on growth, structure, and mechanical properties of sputtered Ti, Al, TiAl, and Ti_3Al films. *Thin Solid Films* **1995**, *270*, 260−263.

(94) Gerlich, D.; Dole, S. L.; Slack, G. A. Elastic properties of aluminum nitride. *J. Phys. Chem. Solids* **1986**, *47*, 437−441.

(95) Jianqiang, H.; Changchun, Z.; Junhua, L.; Yongning, H. Dependence of the resonance frequency of thermally excited microcantilever resonators on temperature. *Sens. Actuators A* **2002**, *101*, 37−41.

(96) Jain, M. K.; Grimes, C. A. Effect of surface roughness on liquid property measurements using mechanically oscillating sensors. *Sens. Actuators A* **2002**, *100*, 63−69.

(97) Daikhin L.; Urbakh, M. Influence of surface roughness on the quartz crystal microbalance response in solution. *Faraday Discuss.* **1997**, *107*, 27−38

(98) Chang, R. F.; Moldover, M. R. High-temperature high-pressure oscillating tube densimeter. *Rev. Sci. Instrum.* **1996**, *67*, 251−256.

(99) Chen, G. Y.; Warmack, R. J.; Huang, A.; Thundat, T. Harmonic response of near-contact scanning force microscopy. *J. Appl. Phys*. **1995**, *78*, 1465−1469.

(100) Nail, T.; Longnire, E. K.; Mantell, S. C. Dynamic response of a cantilever in liquid near a solid wall. *Sens. Actuators A* **2003**, *102*, 240−254.

(101) Harrison, C.; Tavernier, E.; Vancauwenberghe, O.; Donzier, E.; Hsu, K.; Goodwin, A. R. H.; Marty, F.; Mercier, B. On the response of a resonating plate in a liquid near a solid wall. (manuscript in preparation).
(102) Green, C. P.; Sader, J. E. Small amplitude oscillations of a thin beam immersed in a viscous fluid near a solid surface. *Phys. Fluids* **2005**, *17*, 073102-1 to 073102-12.
(103) Ronaldson, K. Mathematical modeling of MEMS densimeters and viscometers. Ph.D. Thesis, University of Southampton, U.K., 2005.
(104) Taylor, G. Flagellar hydrodynamics. *Proc. R. Soc. Ser. A* **1951**, *209*, 447−461.
(105) Hancock, G. J. The self-propulsion of microscopic organisms through liquids. *Proc. R. Soc. Ser. A* **1973**, *217*, 96−121.
(106) Lighthill, J. Flagellar hydrodynamics. *SIAM Rev*, **1976**, *18*, 161−231.
(107) Lighthill, J. Reinterpreting the basic theorem of agellar hydrodynamics. *J. Eng. Math*. **1996**, *30*, 25−34.
(108) Cortez, R. The method of regularized stokeslets. *SIAM J. Sci. Comput.* **2001**, *23*, 1204−1225.
(109) Manrique de Lara, M.; Atkinson, C. Theoretical model on the interaction of a vibrating beam and the surrounding viscous fluid with applications to density and viscosity sensors. *Sensors, 2004*; Proceedings of IEEE, Oct. 24−27, 2004; pp 828−831.
(110) Bourouina, T.; Spirkovitch, S.; Marty, F.; Baillieu, F.; Donzier, E. Silicon etching techniques and application to mechanical devices. *Appl. Surf. Sci*. **1993**, *65*−*66*, 536−542
(111) Manrique de Lara, M. Development of an integrated model of vibrating element fluid property sensor. Ph.D. Thesis, University of London, 2005.
(112) Kovacs, G. T. A.; Maluf, N. I.; Petersen, K. E. Bulk micromachining of silicon. *Proc. IEEE* **1998**, *86*, 1536−1551.
(113) Mehl, J. B. *J. Acoust. Soc. Am.* **1978**, *64*, 1523.
(114) Blom, F. R.; Bouwstra, S.; Elwenspoek, M.; Fluitman, J. H. J. Dependence of the quality factor of micromachined silicon beam resonators on pressure and geometry. *J. Vac. Sci. Technol. B* **1992**, *10*, 19−26.
(115) Yasumura, K. Y.; Stowe, T. D.; Chow, E. M.; Pfafman, T.; Kenny, T. W.; Stipe, B. C.; Rugar, D. Quality factors in micron- and submicron-thick cantilevers. *J. Microelectromech. Syst.* **2000**, *9*, 117−125.
(116) Bruschi, P.; Nannini, A.; Pieri, F. Electrical measurements of the quality factor of microresonators and its dependence on the pressure. *Sens. Actuators A* **2004**, *114*, 21−29
(117) Span, R.; Wagner, W. Equations of state for technical applications. II. Results for nonpolar fluids. *Int. J. Thermophys*. **2003**, *24*, 41−109.
(118) Span, R. *Multiparameter Equations of State: An Accurate Source of Thermodynamic Property Data*; Springer: Berlin, 2000; pp 248, 247, and 255.
(119) Cibulka, I.; Hnedkovský, L. Liquid densities at elevated pressures of *n*-alkanes from C_5 to C_{16}: a critical evaluation of experimental data. *J. Chem. Eng. Data* **1996**, *41*, 657−668.
(120) Cibulka, I. Saturated liquid densities of 1-alkanols from C_1 to C_{10}, and *n*-alkanes from C_5 to C_{16}: a critical evaluation of experimental data. *Fluid Phase. Equilib*. **1993**, *89*, 1−18.
(121) Ambrose, D.; Walton, J. *Pure Appl. Chem*. **1989**, *61*, 1395−1403.
(122) Huber, M. L.; Laesecke, A.; Xiang, H. W. Viscosity correlations for minor constituent fluids in natural gas: *n*-octane, *n*-nonane and *n*-decane. *Fluid Phase Equilib.* **2004**, *224*, 263−270.
(123) Assael, M. J.; Dymond, J. H.; Papadaki, M.; Patterson, P. M. *Int. J. Thermophys*. **1992**, *13*, 269−281.
(124) Tegeler, Ch.; Span, R.; Wagner, W. A new equation of state for argon covering the fluid region for temperatures from the melting line to 700 K at pressures up to 1000 MPa. *J. Phys. Chem. Ref. Data* **1999**, *28*, 779−850.
(125) Lemmon, E. W.; Jacobsen, R. T. Viscosity and thermal conductivity equations for nitrogen, oxygen, argon, and air. *Int. J. Thermophys.* **2004**, *25*, 21−69.
(126) Belonenko, V. N.; Troitsky, V. M.; Belyaev, Yu. E.; Dymond, J. H.; Glen, N. F. Application of a micro-(*p, V, T*) apparatus for measurement of liquid densities at pressures up to 500 MPa. *J. Chem. Thermodyn*. **2000**, *32*, 1203−1219.
(127) Avelino, H. M. T.; Fareleira, J. M. N. A.; Wakeham, W. A. Simultaneous measurement of the density and viscosity of compressed liquid toluene. *Int. J. Thermophys*. **2003**, *24*, 323−336.
(128) Albert, H. J.; Gates, J. A.; Wood, R. H.; Grolier, J.-P. E. Densities of toluene, of butanol and of their binary mixtures from 298 K to 400 K and from 0.5 to 20 MPa. *Fluid Phase Equilib*. **1985**, *20*, 321−30.
(129) Harris, K. R.; Malhotra, R.; Woolf, L. A. Temperature and density dependence of the viscosity of octane and toluene. *J. Chem. Eng. Data* **1997**, *42*, 1254−1260.
(130) Harris, K. R. Temperature and density dependence of the viscosity of toluene. *J. Chem. Eng. Data* **2000**, *45*, 893−897.
(131) Assael, M. J.; Papadaki, M.; Wakeham, W. A. Measurements of the viscosity of benzene, toluene, and *m*-xylene at pressure up to 80 MPa. *Int. J. Thermophys.* **1991**, *12*, 449−457.
(132) Dymond, J. H.; Glen, N. F.; Isdale, J. D.; Pyda, M. The viscosity of liquid toluene at elevated pressures. *Int. J. Thermophys*. **1995**, *16*, 877−882.
(133) Oliveira, C. M. B. P.; Wakeham, W. A. The viscosity of five liquid hydrocarbons at pressures up to 250 MPa. *Int. J. Thermophys*. **1992**, *13*, 773−790.
(134) Dymond, J. H. A.; M. A.; Glen, N. F.; Isdale, J. D. *Int. J. Thermophys.* **1991**, *12* (2), 275−287.
(135) Gouel, P. *Bull. Cent. Rech. Elf Explor. Prod.* **1978**, *2*, 211−225.
(136) Akhundov, T. S.; Abdullaev, F. G. *Izv. Vyssh. Uchebn. Zaved. Neft Gaz* **1970**, *13*, 67−9.
(137) Dymond, J. H.; Malhotra, R.; Isdale, J. D.; Glen, N. F. (*p, ρ, T*) of *n*-heptane, toluene, and oct-1-ene in the range 298 to 373 K and 0.1 to 4430 MPa and representation by the Tait equation. *J. Chem. Thermodyn*. **1988**, *20*, 603−14.
(138) Franck, E. U.; Kerschbaum, S.; Wiegand, G. *Ber. Bunsen-Ges. Phys. Chem*. **1988**, *102*, 1794−1797.
(139) Ihmels, E. C.; Gmehling, J. Densities of toluene, carbon dioxide, carbonyl sulfide, and hydrogen sulfide over a wide temperature and pressure range in the sub- and supercritical state. *Ind. Eng. Chem. Res*. **2001**, *40*, 4470−4477.
(140) Kashiwagi, H.; Hashimoto, T.; Tanaka, Y.; Kubota, H.; Makita, T. Thermal conductivity and density of toluene in the temperature range 273−373 K at pressures up to 250 MPa. *Int. J. Thermophys*. **1982**, *3*, 201−15.
(141) Pöhler, H.; Kiran, E. Volumetric properties of carbon dioxide + toluene at high pressures. *J. Chem. Eng. Data* **1996**, *41*, 482−486.
(142) Verveiko, V. N.; Melnikov, G. A.; Melikhov, Ya. F. *Teplofiz. Svoystva Veshchestv Mater.* **1991**, *30*, 5−16.
(143) Dymond, J. H.; Awan, M. A.; Glen, N. F.; Isdale, J. D. Transport properties of nonelectrolyte liquid mixtures. VIII. Viscosity coefficients for toluene and for three mixtures of toluene + hexane from 25 to 100 °C at pressures up to 500 MPa. *Int. J. Thermophys*. **1991**, *12*, 275−87.
(144) Vieira dos Santos, F. J.; Nieto de Castro, C. A. Viscosity of toluene and benzene under high pressure. *Int. J. Thermophys*, **1997**, *18*, 367−378.
(145) Dymond, J. H.; Robertson, J. Transport properties of nonelectrolyte liquid mixtures. VI. Viscosimetric study of binary mixtures of hexafluorobenzene with aromatic hydrocarbons. *Int. J. Thermophys.* **1985**, *6*, 21−41.
(146) Froba, A. P.; Leipertz, A. *Int. J. Thermophys*. **2001**, *22*, 41−59.
(147) Medani, M. S.; Hasan, M. A. *Can. J. Chem. Eng*. **1977**, *55*, 230−209.
(148) Kaiser, B.; Laesecke, A.; Stelbrink, M. Measurements of the viscosity of liquid toluene in the temperature range 218−378 K. *Int. J. Thermophys.* **1991**, *12*, 289−306.
(149) Caudwell, D. R. Viscosity of dense fluid mixtures. Ph.D. Thesis, University of London, 2004.
(150) Tanaka, Y.; Hosokawa, H.; Kubota, H.; Makita, T. *Int. J. Thermophys*. **1991**, *12*, 245−64.
(151) Dymond, J. H.; Robertson, J.; Isdale, J. D. *Int. J. Thermophys*. **1981**, *2*, 133−154.
(152) Makita, T. Private communication, 1985.
(153) Wong, C.-F.; Hayduk, W. Molecular diffusivities for propene in 1-butanol, chlorobenzene, ethylene glycol, and *n*-octane at elevated pressures. *J. Chem. Eng. Data* **1990**, *35*, 323−328.
(154) Dix, M.; Fareleira, J. M. N. A.; Takaishi, Y. Wakeham, W. A. *Int. J. Thermophys*. **1991**, *12*, 357.
(155) Dymond, J. H.; Robertson, J.; Isdale, J. D. (*p, ρ, T*) of some pure *n*-alkanes and binary mixtures of *n*-atkanes in the range 298 to 373 K and 0.1 to 500 MPa. *J. Chem. Thermodyn*. **1982**, *14*, 51−59.
(156) Bridgman, P. W. *Proc. Am. Acad. Arts Sci*. **1931**, *66*, 185−233.
(157) Kiran, E.; Sen, Y. L. *Int. J. Thermophys*. **1992**, *13*, 411−441.
(158) Sagdeev, D. I.; Mukhamedzyanov, G. Kh. *Teplo-Massoobmen Khim. Tekhnol.* **1977**, *5*, 21.
(159) Banipal, T. S.; Garg, S. K.; Ahluwalia, J. C. *J. Chem. Thermodyn*. **1991**, *23*, 923−931.
(160) Felsing, W. A.; Watson, G. M. The compressibility of liquid *n*-octane. *J. Am. Chem. Soc*. **1942**, *64*, 1822−1823.
(161) Scaife, W. G. S.; Lyons, C. G. R. *Proc. R. Soc. London, Ser. A* **1980**, *370*, 193−211.
(162) Agaev, N. A.; Golubev, I. F. *Gazov. Promst.* **1963**, *8*, 50−53.

Received for review August 16, 2005. Accepted October 21, 2005.

JE0503296